# Metal-insulator transitions and the effects of electron-electron interactions in two-dimensional electron systems

A. A. Shashkin
*Institute of Solid State Physics, Chernogolovka, Moscow District 142432, Russia*

Experimental results on the metal-insulator transitions and the anomalous properties of strongly interacting two-dimensional electron systems are reviewed and critically analyzed. Special attention is given to recent results for the strongly enhanced spin susceptibility and effective mass in low-disordered silicon MOSFETs.

**Contents**



## I. INTRODUCTION

Two-dimensional (2D) electron systems are realized when the electrons are free to move in a plane but their motion perpendicular to the plane is quantized in a confining potential well. At low electron densities in such systems, the strongly-interacting limit is reached because the kinetic energy is overwhelmed by the energy of electron-electron interactions. The interaction strength is characterized by the ratio between the Coulomb energy and the Fermi energy, $r_s^* = E_{ee}/E_F$. Assuming that the effective electron mass is equal to the band mass, the interaction parameter $r_s^*$ in the single-valley case reduces to the Wigner-Seitz radius, $r_s = 1/(\pi n_s)^{1/2} a_B$ and therefore increases as the electron density, $n_s$, decreases (here $a_B$ is the Bohr radius in semiconductor). Possible candidates for the ground state of the system include Wigner crystal characterized by spatial and spin ordering [1], ferromagnetic Fermi liquid with spontaneous spin ordering [2], paramagnetic Fermi liquid [3], etc. In the strongly-interacting limit ($r_s \gg 1$), no analytical theory has been developed to date. According to numeric simulations [4], Wigner crystallization is expected in a very dilute regime, when $r_s$ reaches approximately 35. The refined numeric simulations [5] have predicted that prior to the crystallization, in the range of the interaction parameter $25 \lesssim r_s \lesssim 35$, the ground state of the system is a strongly correlated ferromagnetic Fermi liquid. At higher electron densities, $r_s \sim 1$, the electron liquid is expected to be paramagnetic, with the effective mass, $m$, and Landé $g$ factor renormalized by interactions. Apart from the ferromagnetic Fermi liquid, other intermediate phases between the Wigner crystal and the paramagnetic Fermi liquid may also exist.

In real 2D electron systems, the inherent disorder leads to a drastic change of the above picture, which significantly complicates the problem. According to the scaling theory of localization [6], all electrons in a disordered infinite noninteracting 2D system become localized at zero temperature and zero magnetic field. At finite temperatures, regimes of strong and weak localizations are distinguished: (i) if the conductivity of the 2D electron layer is activated, the resistivity diverges exponentially as $T \to 0$; and (ii) in the opposite limit of weak localization the resistivity increases logarithmically with decreasing temperature — an effect originating from the increased probability of electron scattering from impurities back to the

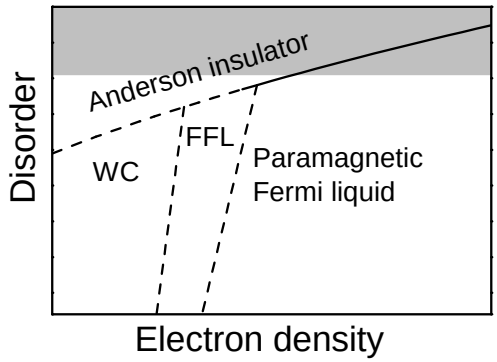


FIG. 1: Schematic phase diagram in disorder vs $n_s$ plane. The Wigner crystal (WC) regime is preceded by the ferromagnetic Fermi liquid (FFL) [5]. The high-disorder region is shaded.

starting point. Interestingly, the incorporation of weak interactions ($r_s < 1$) between the electrons promotes the localization [7]. However, for weak disorder and $r_s \gtrsim 1$ a possible metallic ground state was predicted [8, 9, 10].

In view of the competition between the interactions and disorder, high- and low-disorder limits can be considered. Since many of the experimental groups have made little distinction between these, there has been confusion about interpretation of the data. In highly-disordered electron systems, the range of low densities is not accessible as the strong (Anderson) localization sets in (see Fig. 1). At higher densities, a logarithmic-in-$T$ correction to the resistivity was observed in numerous experiments (see, e.g., Refs. [11, 12, 13]), providing support for the weak localization theory. Apparently, extrapolation of the weak corrections to $T = 0$ is not justified and, therefore, those studies cannot serve as confirmation of the scaling theory. The latter is remarkable by the principal impossibility of experimental verification because all experiments are performed in samples with finite dimensions at finite temperatures. The question whether or not the scaling theory works is essentially a matter of belief.

The case of low-disordered electron systems is much more interesting. Low electron densities corresponding to the strongly-interacting limit become accessible. Experimental results on the metal-insulator phase diagram in perpendicular magnetic fields revealed a close similarity between the insulating phase at low densities and the quantum Hall states. Thus, they excluded the formation of a pinned Wigner crystal in available samples, but supported the existence of a metallic state in zero field [14, 15, 16]. As the magnetic field is decreased, the extended states in the Landau levels were observed to float up in energy relative to the Landau level centers and merge to form a metallic state in the $B = 0$ limit. This contradicts the theoretical scenario that in the limit of zero magnetic field the extended states should float up indefinitely in energy [17, 18] leading to an insulating ground state. The metallic state was found to be remarkable by the strong drop of resistivity with decreasing temperature [19, 20, 21]. Although the origin of the effect was attributed to strong electron-electron interactions, the underlying physics remained unclear until recently.

A breakthrough in understanding this topic occurred in the past four years. After a strongly enhanced ratio $gm$ of the spin and the cyclotron splittings was found at low $n_s$ in silicon MOSFETs [22], it became clear that the system behaves well beyond the weakly interacting Fermi liquid. It was reported that the magnetic field required to produce complete spin polarization, $B_c \propto n_s/gm$, tends to vanish at a finite electron density $n_\chi \approx 8 \times 10^{10}$ cm$^{-2}$, which is close to the critical density, $n_c$, for the metal-insulator transition in this electron system [23, 24, 25]. These findings point to a sharp increase of the spin susceptibility, $\chi \propto gm$, and possible ferromagnetic instability in dilute silicon MOSFETs. In very dilute GaAs/AlGaAs heterostructures, a similar behavior has been observed in both 2D hole and 2D electron systems [26, 27]. Recently, experimental results have indicated that in silicon MOSFETs it is the effective mass, rather than the $g$ factor, that sharply increases at low electron densities [28]. They have also indicated that the anomalous rise of the resistivity with temperature is related to the increased mass. The magnitude of the mass does not depend on the degree of spin polarization, which points to a spin-independent origin of the effective mass enhancement [29, 30]. It is interesting that the observed effects are more pronounced in silicon MOSFETs compared to GaAs/AlGaAs heterostructures, although the fractional quantum Hall effect, which is usually attributed to electron-electron interactions, has not been reliably established in silicon MOSFETs.

The fact that $n_\chi$ is close to the critical density $n_c$ indicates that the metal-insulator transition in silicon samples with very low disorder potential is a property of a clean 2D system and is driven by interactions [23]. This is qualitatively different from a localization-driven transition in more-disordered samples that occurs at appreciably higher densities than $n_\chi$ which are also dependent on disorder strength. In this review, attention is focused on results obtained in the clean regime.

There are several good reviews on the topic in question (see, e.g., Refs. [31, 32]). However, they have either become outdated or do not express criticism toward the items of general belief, e.g., the scaling theory. Below, I describe the main experimental results and give a broad view on the metal-insulator transition and anomalous properties of 2D electron systems at low densities.

## II. METAL-INSULATOR PHASE DIAGRAMS IN A MAGNETIC FIELD

Metal-insulator transitions in perpendicular magnetic fields attracted a great deal of interest in the past decade. The experimental activity was strongly stim-

ulated by theoretical predictions that Wigner crystallization is promoted in the presence of a magnetic field [33, 34, 35, 36, 37]. The insulating phase at low electron densities was mainly studied whose origin was attributed to possible formation of the Wigner crystal [38, 39, 40, 41, 42, 43, 44, 45, 46, 47, 48, 49, 50, 51, 52]. However, the latter has been precluded in studies of the metal-insulator phase diagram including quantum Hall states, which show a close similarity of all insulating phases in available samples [14, 15, 16]. It is interesting that there are some firmly-established experimental results which have not attracted much of the theorists' attention. These include (i) oscillations of the metal-insulator phase boundary as a function of perpendicular magnetic field; and (ii) finite bandwidth of the extended states in the Landau levels.

### A. Floating-up of the extended states in perpendicular magnetic fields

#### 1. *First observation*

The scaling theory of localization was challenged by the quantum Hall effect (quantization of the Hall resistivity, $\rho_{xy} = h/\nu e^2$, at integer filling factor $\nu$ accompanied with vanishing longitudinal resistivity, $\rho_{xx}$) [53] which implies the existence of extended states in the Landau levels (see section II C). To reconcile these two, it was theoretically predicted almost immediately that the extended states in the Landau levels cannot disappear discontinuously with decreasing magnetic field but must float up indefinitely in energy in the limit of $B = 0$ [17, 18]. The expected phase diagram is shown in the inset to Fig. 2(a). An equivalent diagram plotted in disorder versus inverse filling factor ($1/\nu = eB/hcn_s$) plane is known as the global phase diagram for the quantum Hall effect [54]. As long as no merging of the extended states was considered to occur, their piercing of the Fermi level was predicted to cause quantization of the Hall conductivity in weak magnetic fields [55, 56].

The first attempt [14] to experimentally determine the metal-insulator phase diagram at low temperatures in low-disordered silicon MOSFETs already revealed discrepancies with the theory (see Fig. 2(a)). In that paper, a somewhat arbitrary criterion for the longitudinal conductivity, $\sigma_{xx} = e^2/20h$, was used to map out the phase boundary that corresponds to the Anderson transition to the regime of strong localization. However, firstly, the phase boundary was shown to be insensitive to the choice of the cutoff value (see, e.g., Ref. [57]), and secondly, that particular cutoff value is consistent with the results obtained for quantum Hall states by a vanishing activation energy combined with a vanishing nonlinearity of current-voltage characteristics when extrapolated from the insulating phase [15] (note that for the lowest-density phase boundary, a lower value $\sigma_{xx}^{-1} \approx 100\,\mathrm{kOhm}$ at a temperature $\approx 25$ mK follows from the latter method). The

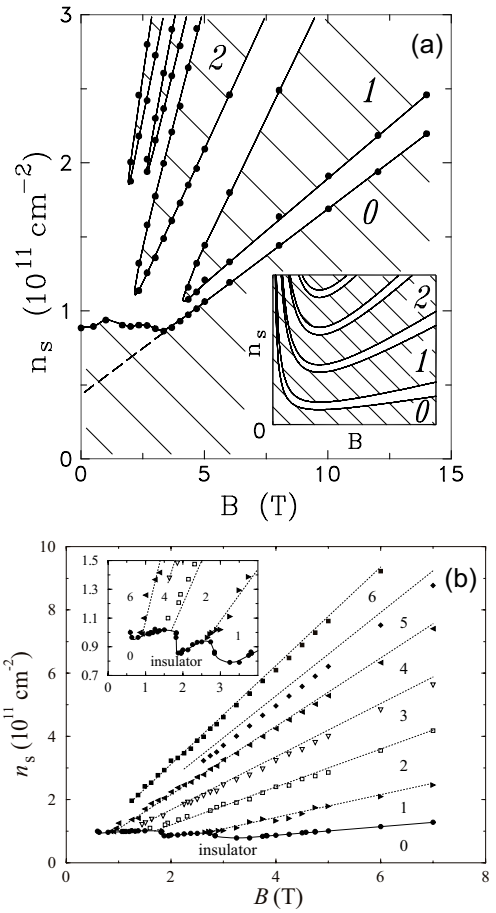


FIG. 2: (a) Metal-insulator phase diagram in a low-disordered 2D electron system in silicon MOSFETs obtained using a cutoff criterion, $\sigma_{xx} = e^2/20h$, at a temperature $\approx 25$ mK. The dimensionless $\sigma_{xy}h/e^2$ in different insulating phases is indicated. The slope of the dashed line is close to $e/2hc$. A sketch of the expected phase diagram is displayed in the inset. From Ref. [14]. (b) The map of extended states determined by maxima in $\sigma_{xx}$ in a low-disordered silicon MOSFET. Numbers show $\sigma_{xy}$ in units of $e^2/h$. Adopted from Ref. [58].

metallic phase surrounds each insulating phase as characterized by the dimensionless Hall conductivity, $\sigma_{xy}h/e^2$, that counts the number of quantum levels below the Fermi level (in bivalley (100)-silicon MOSFETs, spin and valley degeneracies of the Landau level should be taken into account). This indicates that the extended states indeed do not disappear discontinuously. However, with decreasing magnetic field they float up in energy relative to the Landau level centers and merge forming a metallic state in the limit of $B = 0$ (see sections II B and II D). Besides, the phase boundary at low electron densities oscillates as a function of $B$ with minima corresponding to integer filling factors. The phase boundary oscillations manifest themselves in that at electron densities near the $B = 0$ metal-insulator transition, the magnetoresistance oscillates with an amplitude that diverges as

$T \to 0$ [38]; the regions in which the magnetoresistance diverges are referred to as reentrant insulating phase (see section II B).

### 2. Other methods and 2D carrier systems

The topology of the observed metal-insulator phase diagram — merging the extended states and, hence, the presence of direct transitions between the insulating phase with $\sigma_{xy} = 0$ and quantum Hall phases with $\sigma_{xy}h/e^2 > 1$ — is robust being insensitive to the method for spotting the phase boundary [15, 58] and to the choice of 2D carrier system [59, 60]. It was verified using a criterion of vanishing activation energy and vanishing nonlinearity of current-voltage characteristics as extrapolated from the insulating phase, which allows more accurate determination of the Anderson transition [15]. Kravchenko et al. [58] also applied for similar silicon MOSFETs a method that had been suggested in Ref. [61]. They studied extended states by tracing maxima in the longitudinal conductivity in the $(B, n_s)$ plane (see Fig. 2(b)) and found a good agreement with the aforementioned results. A similar merging of at least the two lowest extended states was observed in more-disordered 2D hole systems in a GaAs/AlGaAs heterostructure [59] (see Fig. 3(a)) and in a Ge/SiGe quantum well [60] (see Fig. 3(b)). In the former case the extended states were determined by peaks in $\sigma_{xx}$ or temperature-independent crossing points in $\rho_{xx}$; in the latter they were associated either with maxima in $\rho_{xx}$ and/or $d\rho_{xy}/dB$, or with crossing points of $\rho_{xx}$ at different temperatures. It is noteworthy that a bad combination of the criterion for determining the phase boundary and the 2D carrier system under study may lead to a failure of mapping out the phase diagram down to relatively weak magnetic fields. In Ref. [61], extended states were studied by measuring maxima in the longitudinal conductivity in the $(B, n_s)$ plane for the strongly-disordered 2D electron system in GaAs/AlGaAs heterostructures (see Fig. 3(c)). Because of strong damping of the Shubnikov-de Haas oscillations in low magnetic fields, the desired region on the phase diagram below 2 T was not accessible in that experiment. This invalidates the claim of Glozman et al. [61] that the extended states do not merge [62]. The behavior of the lowest extended state in Fig. 3(c), which Glozman et al. [61] claim to float up above the Fermi level as $B \to 0$, simply reflects the occurrence of a phase boundary oscillation minimum at filling factor $\nu = 2$, similar both to the minimum at $\nu = 1$ in Fig. 3(a) and to the case of silicon MOSFETs (Fig. 2). Such a minimum manifests itself in that there exists a minimum in $\rho_{xx}$ at integer $\nu \geq 1$ that is straddled by the insulating phase [38, 63, 64, 65, 66, 67]. To this end, all available data for the metal-insulator phase diagrams agree well with each other, except those in the vicinity of $B = 0$. In weak magnetic fields, experimental results obtained in 2D electron systems with high disorder are not method-independent. Glozman et al. [61] found that

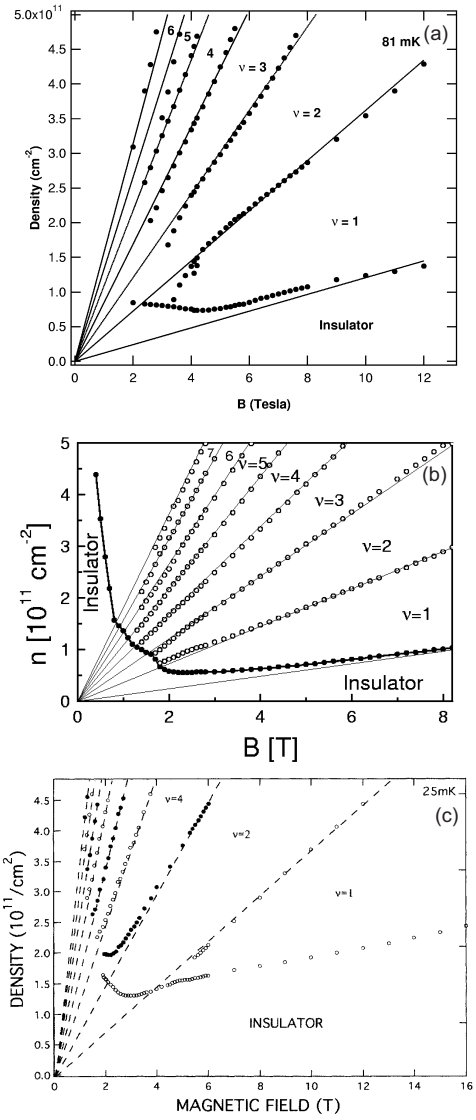


FIG. 3: (a) A map of the extended states for a highly-disordered 2D hole system in GaAs/AlGaAs heterostructures. Each data point represents a distinct peak in $\sigma_{xx}$ or a temperature independent crossing point in $\rho_{xx}$. Numbers show the value of $\sigma_{xy}h/e^2$. Adopted from Ref. [59]. (b) A map of the extended states for a highly-disordered 2D hole system in a Ge/SiGe quantum well. The open circles represent maxima in $\rho_{xx}$ and/or $d\rho_{xy}/dB$. The solid circles correspond to crossing points of $\rho_{xx}$ at different temperatures. Numbers show the value of $\sigma_{xy}h/e^2$. Adopted from Ref. [60]. (c) Behavior of the extended states determined by maxima in $\sigma_{xx}$ in a strongly-disordered 2D electron system in GaAs/AlGaAs heterostructures. Numbers show $\sigma_{xy}$ in units of $e^2/h$. Adopted from Ref. [61].

the cutoff criterion yields basically a flat phase boundary towards $B = 0$, which is in agreement with the data for silicon MOSFETs (Fig. 2(a)). On the contrary, Hilke et al. [60] employed the method based on temperature dependences of $\rho_{xx}$ and obtained a turn up on the phase boundary in Fig. 3(b). Note that the validity of the data

for the lowest extended state at magnetic fields $\lesssim 1.5$ T in Fig. 3(b) is questionable because the weak temperature dependences of $\rho_{xx}$ as analyzed by Hilke et al. [60] cannot be related to either an insulator or a metal. The same applies to similar temperature dependences observed, e.g., in Refs. [68, 69, 70, 71, 72, 73, 74].

### *3. Weak-field regime*

As a matter of fact, the weak-field problem — whether or not there is an indefinite rise of the phase boundary as $B \to 0$ — is a problem of the existence of a metal-insulator transition at $B = 0$ and $T = 0$. In dilute 2D electron systems with low enough disorder, the resistivity, $\rho$, strongly drops with lowering temperature providing an independent way of facing the issue. Given strong temperature dependences of $\rho$, those with $d\rho/dT > 0$ ($d\rho/dT < 0$) can be associated with a metallic (insulating) phase [19, 20, 21, 75, 76]. If extrapolation of the temperature dependences of $\rho$ to $T = 0$ is valid, the curve with $d\rho/dT = 0$ should correspond to the metal-insulator transition. The fact that this method and the one, based on a vanishing activation energy combined with a vanishing nonlinearity of current-voltage curves when extrapolated from the insulating phase, give equivalent results strongly supports the existence of a true metal-insulator transition in zero magnetic field [77] (see section II D). As long as in more-disordered 2D carrier systems the metallic ($d\rho/dT > 0$) behavior is suppressed (see, e.g., Refs. [78, 79, 80, 81, 82, 83, 84, 85]) or disappears entirely, it is definitely incorrect to extrapolate those weak temperature dependences of $\rho$ to $T = 0$ with the aim to distinguish between insulator and metal. Once one of the two methods fails, it remains to be seen how to verify the conclusion as inferred from the other method. This makes uncertain the existence of a true $B = 0$ metal-insulator transition in 2D electron systems with high disorder.

### *4. Phase boundary oscillations*

The next important point is the oscillating behavior of the phase boundary that restricts the insulating phase with $\sigma_{xy} = 0$ (see, e.g., Fig. 2). It is worth noting that the oscillations persist down to the magnetic fields corresponding to the fillings of higher Landau levels, as indicated also by magnetoresistance oscillations [38, 63, 67]. The oscillation period includes the following elements. With decreasing magnetic field the lowest extended states follow the Landau level, float up in energy relative to its center, and merge with extended states in the next quantum level. The last element was absent in the original considerations [17, 18, 54, 55] leading to discrepancies between experiment and theory. Recently, theoretical efforts have been concentrated on modifications of the global phase diagram for the quantum

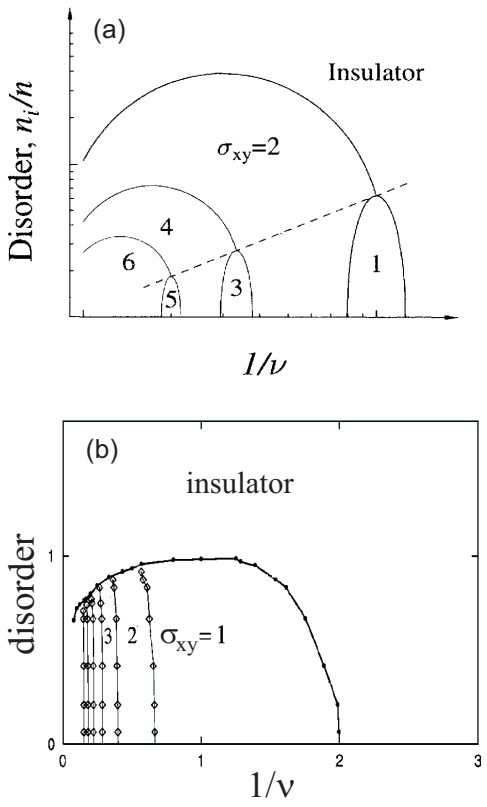


FIG. 4: (a) A sketch of the modified global phase diagram for the quantum Hall effect as expected from the mean-field approximation neglecting the Zeeman energy. The dashed line corresponds to the collapse of the exchange-enhanced spin splitting. Adopted from Ref. [86]. (b) Numerical results for the phase diagram within a tight-binding model. Adopted from Ref. [103].

Hall effect to reach topological compatibility with the observed metal-insulator phase diagram. It has been predicted that the spin-up and spin-down extended states in the Landau level should merge [86, 87] (see Fig. 4(a)). However, in view of lowest extended states, the topology of the phase diagram changes for the lowest Landau level only; besides, they do not float up before merging. It has been verified that shifts of the extended states from the Landau level centers that are caused by disorder-induced mixing of the Landau levels are small [88, 89, 90, 91, 92, 93]. Within tight-binding models, an indication had been first obtained that the extended states disappear [94, 95, 96], which caused some criticism toward the relevance of such a lattice model to the continuum system [97, 98]. After that, floating up of the extended states without merging has been found in studies [99, 100, 101]. In contrast, Sheng and Weng [102, 103] have obtained a merging of the extended states although without an oscillating behavior of the lowest extended states (see Fig. 4(b)). As for now, the effect of the phase boundary oscillations is still far from being described theoretically.

Concluding this section, I would like to make a couple of remarks on alternative ways for determining the metal-insulator phase boundary. An attempt was made to spot the phase boundary in the limit of $B = 0$ using a criterion of $\sigma_{xy} = e^2/2h$ [104]. However, that particular value of $\sigma_{xy}$ has no special meaning as $B \to 0$. An idea was expressed to relate the minimum in the inverse compressibility to the metal-insulator transition [105]. However, it has been recently shown that in zero magnetic field, this minimum lies at carrier densities well above the critical density for the percolation metal-insulator transition [106]. Particularly, in highly-disordered 2D carrier systems, its position may be close to that of the crossing point of the resistivity at different temperatures [105] which formally yields overestimated densities for the metal-insulator transition because of suppression of the metallic behavior (see section II D).

### B. Similarity of the insulating phase and quantum Hall phases

#### 1. *Method for comparison and consequences*

About a decade ago, main attention was paid to the insulating phase at low electron densities as a possible candidate for the Wigner crystal. It was argued that its aforementioned reentrant behavior is a consequence of the competition between the quantum Hall effect and the pinned Wigner crystal [38, 39]. Another certain argument was strongly nonlinear current-voltage characteristics in the insulating phase which were attributed to depinning of the Wigner crystal [40, 41]. Similar features of the insulating phase in a 2D electron (near $\nu = 1/5$) [42, 43, 44, 45, 46, 47, 48, 49] and 2D hole (near $\nu = 1/3$) [50, 51, 52] systems in GaAs/AlGaAs heterostructures with relatively low disorder were also attributed to a pinned Wigner crystal which is interrupted by the fractional quantum Hall state. An alternative scenario was discussed in terms of percolation metal-insulator transition [57, 107, 108]. To distinguish between the two scenarios, the behavior of activation energy and current-voltage characteristics in the insulating phase was studied and compared to that in quantum Hall phases [15, 16, 109].

In contrast to the low-density insulating phase, the way of determining the current-voltage characteristics of the quantum Hall phases is different for Corbino and Hall bar geometries. In the former the dissipationless Hall current does not contribute to the dissipative current that is proportional to $\sigma_{xx}$, allowing straightforward measurements of current-voltage curves for all insulating phases. In the latter the two current channels are connected through edge channels (see section II C), and current-voltage characteristics correspond to quantum-Hall-effect breakdown curves. The dissipative backscattering current, $I$, that flows between opposite edge channels is balanced by the Hall current in the filled Landau

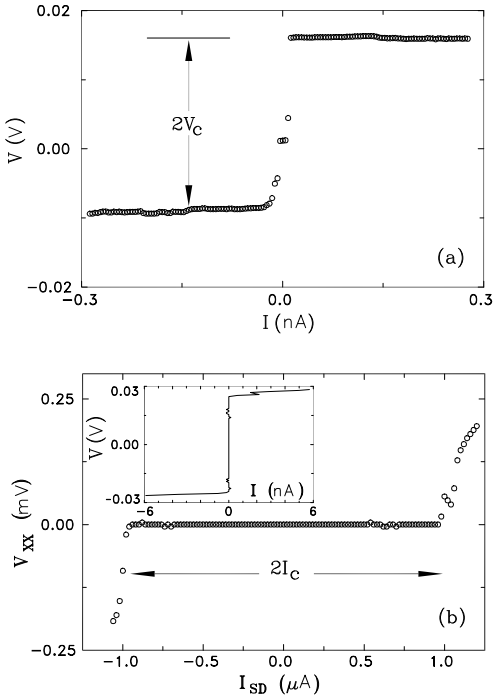


FIG. 5: Current-voltage characteristics in a low-disordered silicon MOSFET in $B = 12$ T at $T \approx 25$ mK for the low-density insulating phase at $n_s = 1.74 \times 10^{11}$ cm$^{-2}$ (a) and the insulating phase with $\sigma_{xy}h/e^2 = 1$ at $n_s = 2.83 \times 10^{11}$ cm$^{-2}$ (b). In (b) the measured breakdown dependence $V_{xx}(I_{sd})$ is converted into current-voltage characteristics (inset). From Ref. [15].

levels associated with the longitudinal voltage, $V_{xx}$. As long as $\sigma_{xx} \ll \sigma_{xy}$, the quantized value of $\sigma_{xy}$ is a factor that allows determination of $I = \sigma_{xy}V_{xx}$ and the Hall voltage, $V = I_{sd}/\sigma_{xy}$, from the experimental breakdown dependence of $V_{xx}$ on source-drain current, $I_{sd}$. The dependence $V(I)$ is a current-voltage characteristic, which is equivalent to the case of Corbino geometry [15] (see Fig. 5). Not only are the current-voltage curves similar for all insulating phases, but they behave identically near the metal-insulator phase boundaries (see Fig. 6(a)). The dependence of the critical voltage, $V_c$, on the distance from the phase boundary is close to a parabolic law [41, 57]. The phase boundary position determined by a vanishing $V_c$ is practically coincident with that determined by a vanishing activation energy, $E_a$, of electrons from the Fermi level $E_F$ to the mobility edge, $E_c$ (see Fig. 6(b)). The value $E_a$ is determined from the temperature dependence of the conduction in the linear interval of current-voltage curves, which is activated at not too low temperatures [110]; note that it transforms into variable range hopping as $T \to 0$ (see below). The activation energy changes linearly with the distance from the phase boundary reflecting constancy of the thermodynamic density of states near the transition point (see also section II D). The threshold behavior of the current-

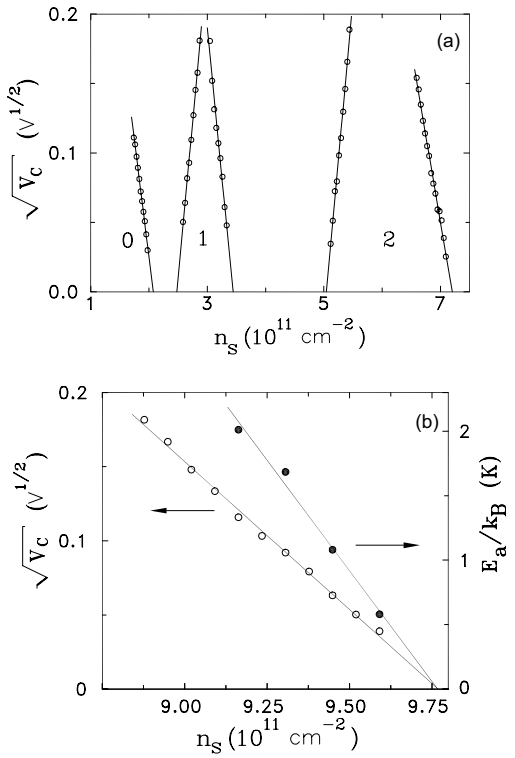


FIG. 6: (a) Square root of the critical voltage as a function of electron density at the phase boundaries corresponding to $\sigma_{xy}h/e^2 = 0$, 1, and 2 in $B = 12$ T for a low-disordered 2D electron system in silicon MOSFETs. (b) Behavior of the critical voltage and the activation energy near the phase boundary in $B = 16$ T. From Ref. [15].

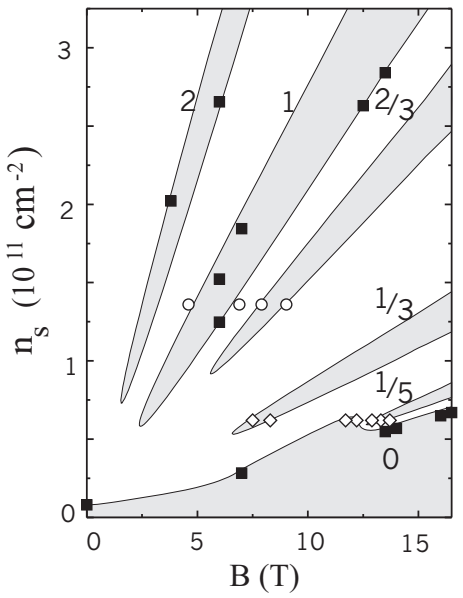


FIG. 7: Metal-insulator phase diagram in a relatively low-disordered 2D electron system in GaAs/AlGaAs heterostructures. The points corresponding to phase boundaries are obtained on two samples using a criterion of vanishing activation energy and vanishing nonlinearity of current-voltage curves as extrapolated from the insulating phase (circles and squares) and on one sample from Ref. [113] using a cutoff criterion, $\sigma_{xx}^{-1} = 10$ MOhm, at a temperature $\approx 25$ mK as follows from the former method (diamonds). The solid lines are guides to the eye. Digits indicate $\sigma_{xy}h/e^2$ for different insulating phases. From Ref. [16].

voltage characteristics is caused by the breakdown in the insulating phases. The breakdown occurs when the localized electrons at the Fermi level gain enough energy to reach the mobility edge in an electric field, $V_c/d$, over a distance given by the localization length, $L$ [15, 111]:

$$eV_cL/d = |E_c - E_F|, \qquad (1)$$

where $d$ is the corresponding sample dimension. The values $E_a$ and $V_c$ are related through the localization length which is temperature independent and diverges near the transition as $L(E_F) \propto |E_c - E_F|^{-s}$ with exponent $s$ close to unity, in agreement with the theoretical value $s = 4/3$ in classical percolation problem [112]. The value of the localization length is practically the same near all metal-insulator phase boundaries, which indicates that even quantitatively, all insulating phases are very similar. Note that since the localization length in Eq. (1) is small compared to the sample sizes, the phase boundary position determined by the diverging localization length refers to an infinite 2D system. As inferred from the vanishing of both $E_a$ and $V_c$ at the same point (see Fig. 6(b)), possible shifts of the mobility threshold due to finite sample dimensions are small, which justifies extrapolations to the limit of $L \to \infty$.

The consequences of the method include (i) as long as there occurs no dramatic change in transport properties, this excludes the pinned Wigner solid as the origin for the insulating phase at low electron densities in available samples of low-disordered silicon MOSFETs; (ii) the metal-insulator phase diagram of Fig. 2(a) is verified and substantiated; (iii) the existence of a metal-insulator transition in zero magnetic field is supported (see section II D); and (iv) the bandwidth of the extended states in the Landau levels is finite. All of these are also valid for relatively low-disordered 2D carrier systems in GaAs/AlGaAs heterostructures with a distinction that fractional quantum Hall phases are involved. Yet, the topology of the phase diagram remains unchanged including the oscillating behavior of the phase boundary that restricts the low-density insulating phase (see Fig. 7). Additional confirmation of the percolation transition to the low-density insulating phase in GaAs/AlGaAs heterostructures was obtained by studies of the high-frequency conductivity [113] and time-resolved photoluminescence of 2D electrons [114], as discussed in Ref. [16].

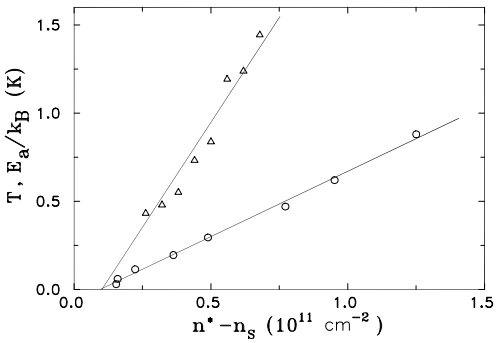


FIG. 8: Temperature dependence of the $\rho_{xx}$ peak width ($n^* - n_s$) at half of the peak height counted from $n^*$ corresponding to $\nu^* = 2.5$ (circles) and the behavior of the activation energy (triangles) in a low-disordered silicon MOSFET in $B = 14$ T. From Ref. [15].

### 2. *Finite bandwidth of extended states*

It was predicted two decades ago that the localization length diverges as a power law at a single energy, $E^*$, which is the center of the Landau level [115, 116, 117]: $L(E) \propto |E - E^*|^{-s}$. An idea to check this prediction based on low-temperature measurements of $\sigma_{xx}$ [118] was quickly developed to a concept of single-parameter scaling [119]. It was suggested that the magnetoresistance tensor components are functions of a single variable that is determined by the ratio of the dephasing length, $L_d(T) \propto T^{-p/2}$ (where $p$ is the inelastic-scattering-time exponent), and the localization length. The concept was claimed to be confirmed by measurements of temperature dependences of the peak width, $\Delta B$, in $\rho_{xx}$ (or $\sigma_{xx}$) and the maximum of $d\rho_{xy}/dB$ in a highly-disordered 2D electron system in InGaAs/InP heterostructures, which yielded $\Delta B \propto T^{\kappa}$, where $\kappa = p/2s \approx 0.4$ [120]. Later, both deviations in the power law and different exponents in the range between $\kappa = 0.15$ and $\kappa = 1$ were observed for other 2D carrier systems, different Landau levels, and different disorder strengths [65, 68, 69, 121, 122, 123, 124, 125, 126, 127, 128, 129, 130, 131, 132, 133, 134, 135, 136, 137, 138, 139, 140]. Importantly, the scaling analysis of experimental data in question is based on two unverified assumptions: (i) zero bandwidth of the extended states in the Landau levels; and (ii) constancy of the thermodynamic density of states in the scaling range. If either assumption is not valid, this may lead at least to underestimating the experimental value of exponent $\kappa$.

The method of vanishing activation energy and vanishing nonlinearity of current-voltage characteristics as extrapolated from the insulating phase shows that the former assumption is not justified. Moreover, measurements of the peak width in $\rho_{xx}$ as a function of temperature in low-disordered silicon MOSFETs yield a linear dependence which extrapolates as $T \to 0$ to a finite peak width, accordingly [15] (see Fig. 8). Very similar temperature (and frequency) dependences were observed in highly-disordered 2D carrier systems in GaAs/AlGaAs heterostructures [141, 142] and Ge/SiGe heterostructures [66, 143]. It is noteworthy that a similar behavior is revealed if the data from the publications, which claim the observation of scaling, is plotted on a linear rather than logarithmic scale (see, e.g., Fig. 9); finite values of the peak width as $T \to 0$ are even more conspicuous for the data of Refs. [123, 124, 125]. The reason for the ambiguity is quite simple: within experimental uncertainty, it is difficult (on a logarithmic scale it is especially difficult) to distinguish between sublinear/superlinear fits to the data and linear fits which do not have to run to the origin.

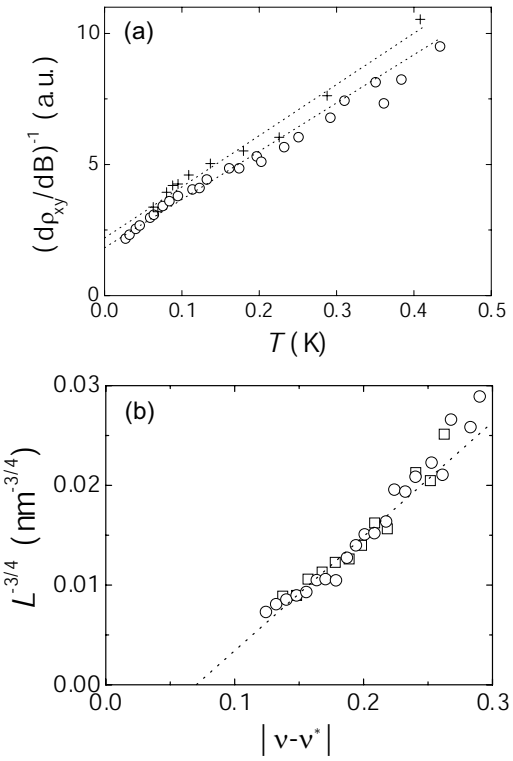


FIG. 9: (a) Temperature dependence of the $\rho_{xx}$ peak width as determined by the maximum $d\rho_{xy}/dB$ at $\nu^* = 1.5$ in a highly-disordered 2D electron system in GaAs/AlGaAs heterostructures. Different symbols correspond to different runs. The dashed lines are linear fits to the data. Adopted from Ref. [126]. (b) Localization length, determined by the high-frequency conductivity in the variable-range-hopping regime in a highly-disordered 2D electron system in GaAs/AlGaAs heterostructures, as a function of the filling factor deviation from $\nu^* = 2.5$ (squares) and $\nu^* = 3.5$ (circles) towards the $\nu = 3$ plateau. The dashed line is a linear fit that is expected from classical percolation approach with exponent $s = 4/3$. Adopted from Ref. [138].

Although lack of data in most of the above experimental papers does not allow one to verify the validity of both assumptions, it is very likely that there is no qualitative difference between all of the discussed results. As

a matter of fact, they can be described by a linear (or weakly sublinear) temperature dependence with a finite offset at $T = 0$. Here comes an alternative and simple explanation of the temperature dependence of the peak width in $\rho_{xx}$ in terms of thermal broadening. Within percolation picture, if the activation energy $E_a \sim k_B T$, the conduction is order of the maximum $\sigma_{xx}$ so that the value of $\sim k_B T$ gives a thermal shift of the effective mobility edge corresponding to the $\sigma_{xx}$ peak width [15]. Despite the concept of thermal broadening has been basically ignored in the literature in search for less trivial data interpretations, it looks as if no experimental results go beyond this favoring the concept of single-parameter scaling. Once the behavior of the localization length is not reflected by the temperature-dependent peak width in $\rho_{xx}$, no experimental support is provided for numeric calculations of the localization length which give a somewhat larger exponent $s \approx 2$ compared to $s = 4/3$ in classical percolation problem (see, e.g., Ref. [144]). The latter value of $s$ as well as the behavior of the localization length in Fig. 6 have been recently confirmed by measurements of the high-frequency conductivity in the variable-range-hopping regime [138] (see Fig. 9(b)).

Thus, the finding of finite bandwidth of the extended states in the Landau levels [15, 16], which is in obvious contradiction to scaling arguments, is a firmly-established experimental result. Curiously, it has got no theoretical considerations for ten years.

#### *3. Hall insulator*

Deep in the insulating phases and at low temperatures the variable-range-hopping regime occurs in which the conductivity $\sigma_{xx}$ is small compared to its peak value [112]. In this regime it was predicted that the deviation, $\Delta\sigma_{xy}$, of $\sigma_{xy}$ from its quantized value in strong magnetic fields is much smaller than $\sigma_{xx} \propto \exp(-(T_0/T)^{1/2})$ [145]: $\Delta\sigma_{xy} \propto \sigma_{xx}^{\gamma}$ with exponent $\gamma \approx 1.5$; note that this is in contrast to a straightforward linear relation in the activation regime, as inferred from approximately the same behavior with temperature of the $\rho_{xx}$ peak width and the maximum of $d\rho_{xy}/dB$. Later, finite $\rho_{xy}$ contrasted by diverging $\rho_{xx}$ was found in calculations of the $T = 0$ magnetotransport coefficients in the insulating phase with vanishing $\sigma_{xx}$ and $\sigma_{xy}$ [146, 147]. Such a behavior of $\rho_{xx}$ and $\rho_{xy}$ indicates a special quadratic relation between conductivities

$$\sigma_{xy} \propto \sigma_{xx}^2. \qquad (2)$$

Moreover, it was shown that $\rho_{xy}$ is close to the classical value $(B/n_s ec)$ [148] providing arguments for the existence of a Hall insulator phase [54].

Values $\rho_{xy}$ close to $B/n_s ec$ were experimentally found in the low-density insulating phase, deviations from the classical Hall line being attributed to possible admixture of $\rho_{xx}$ [43, 63, 149, 150, 151, 152, 153, 154]. Thus, the distinction of the Hall insulator phase from the quantum Hall phases — the absence of extended states below the Fermi level — becomes evident when expressed in terms of $\rho_{xx}$ and $\rho_{xy}$.

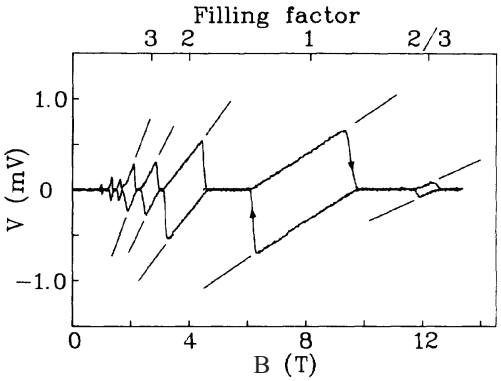


FIG. 10: The induced voltage in a Corbino sample of a GaAs/AlGaAs heterostructure in up- and down-sweeps of the magnetic field. Also shown by straight lines are the expected slopes for $\nu = 2/3$, 1, 2, 3, and 4. From Ref. [168].

It was empirically found in low-disordered silicon MOSFETs that the lowest-filling-factor peak in $\sigma_{xx}$ plotted in the $(\sigma_{xy}, \sigma_{xx})$ plane is close to a semicircle centered at $(e^2/2h, 0)$ [39, 108, 154]. The semicircle law for the lowest-$\nu$ peak was reproduced in a highly-disordered 2D hole system in a Ge/SiGe quantum well [72, 73]. There, it was shown that the semicircle relation originates directly from conductivity/resistivity tensor inversion

$$\sigma_{xx}^2 + \left(\sigma_{xy} - \frac{e^2}{2h}\right)^2 = \left(\frac{e^2}{2h}\right)^2 + \frac{1 - \rho_{xy} e^2/h}{\rho_{xx}^2 + \rho_{xy}^2}, \qquad (3)$$

because the (narrow) $\sigma_{xx}$ peak in question is located at filling factor just below $\nu = 1$ (see, e.g., Fig. 2) where $\rho_{xy}$ is still close to $h/e^2$. Although this finding is consistent with theories [155, 156, 157, 158, 159], the semicircle law does not seem universal if higher-$\nu$ peaks in $\sigma_{xx}$ with different heights are involved [39, 123, 154, 160].

### C. Edge channel effects, direct measurements of the quantized Hall conductivity

In a magnetically quantized 2D electron system, the Landau levels bend up at the sample edges due to the confining potential, and edge channels are formed where these intersect the Fermi energy (see, e.g., Ref. [161]). There rises a natural question whether the current in the quantum Hall state flows in the bulk or at the edges of the sample. Although the Hall conductivity $\sigma_{xy}$ was not directly measured in early experiments on the quantum Hall effect, it seemed obvious that this value corresponds to $\rho_{xy}$, in agreement with the concept of currents that flow in the bulk [162]; that stands to reason that finite $\sigma_{xy}$ would give evidence for the existence of extended states in the Landau levels [155, 161]. This concept was

challenged by the edge current model [163]. In the latter approach extended states in the bulk are not crucial and the problem of current distributions in the quantum Hall effect is reduced to a one-dimensional task in terms of transmission and reflection coefficients as defined by the backscattering current at the Fermi level between the edges. Importantly, if the edge current contributes significantly to the net current, conductivity/resistivity tensor inversion is not justified, because the conductivities $\sigma_{xx}$ and $\sigma_{xy}$ are related to the bulk of the 2D electron system.

To verify whether or not the Hall conductivity is quantized, direct measurements of $\sigma_{xy}$ were necessary excluding a possible shunting effect of the edge currents. Being equivalent to Laughlin's gedanken experiment [164, 165], such measurements were realized using the Corbino geometry which allows separation of the bulk contribution to the net current [166, 167, 168, 169, 170, 171, 172, 173]. A Hall charge transfer below the Fermi level between the coasts of a Corbino sample is induced by magnetic field sweep through the generated azimuthal electric field. If $\sigma_{xx} \to 0$, no discharge occurs allowing determination of the transferred charge,

$$Q = \sigma_{xy}\pi r_{\rm eff}^2 c^{-1}\delta B, \qquad (4)$$

where $r_{\rm eff}$ is the effective radius. The induced voltage, $V = Q/C$, which is restricted due to a large shunting capacitance, $C$, changes linearly with magnetic field with a slope determined by $\sigma_{xy}$ in the quantum Hall states until the dissipationless quantum Hall state breaks down (see Fig. 10). The fact that the quantization accuracy of $\sigma_{xy}$ (about 1%) is worse compared to $\rho_{xy}$ may be attributed to non-constancy of the effective area in not very homogeneous samples. Thus, the Hall current in the quantum Hall effect flows not only at the edges but also in the bulk of the 2D electron system through the extended states in the filled Landau levels.

Apparently, the dissipative backscattering current in Hall bar samples should be balanced by Hall current in the filled Landau levels resulting in a longitudinal potential drop [174]. This point makes significant contribution to the edge current model.

From an experimental viewpoint, all edge channel effects proceed from slow equilibration (at macroscopic distances) between the electrochemical potentials of different edge states including the state in the bulk. As long as such an equilibration occurs at the edges at the Fermi level, the applicability of the edge state model is justified. The approach accounts for effects observed in conventional transport experiments, which include the nonlocal resistance and the effects related to contacts/reservoirs (see, e.g., Ref. [175]). However, particular potential profiles at the edge and current distributions can be probed only using non-destructive spatially-resolved imaging techniques [176, 177, 178, 179, 180, 181, 182, 183, 184, 185, 186, 187, 188, 189, 190, 191, 192, 193, 194]; note that many of the so-revealed inhomogeneous samples show quite good magnetotransport characteristics. Contrary to standard considerations of the edge channels in terms of skipping orbits for a confining potential that is sharp on the magnetic length, $l_B = (\hbar c/eB)^{1/2}$, it turns out that in most samples the potential profile at the edge is smooth and spans over much larger distances than $l_B$. Edge regions corresponding to the scale of confining potential $\approx 10$ $\mu$m were visualized in Hall photovoltage optical imaging experiments on standard Hall bar samples [183] (see Fig. 11(a)). Since the Hall electric field is nearly constant, even if some field enhancement occurs near the edges [176], the edge current contribution can be appreciable depending on a particular sample.

For a soft confining potential, edge channels are also referred to as compressible and incompressible strips whose spacing is determined by the electron density gradient [195]. This is very similar to the long-standing phenomenon of Hall current pinch: given electron density gradients, the Hall current basically flows in narrow channels (or incompressible strips) determined by the minimum $\sigma_{xx}$, their position in the sample being controlled, e.g., by magnetic field [181, 182, 196, 197, 198, 199]. When located at the edge, the pinch of Hall current becomes identical with the subject of Ref. [195]. The Hall current channels at the edge were imaged using a single-electron transistor as a probe for the local $\sigma_{xx}$ [184] (see Fig. 11(b)). Applying a negative voltage to a side gate leads to a shift of the edge of the 2D electron system towards the probe, thereby creating a line scan of the local $\sigma_{xx}$ across the sample edge. Vanishing $\sigma_{xx}$ is indicated by enhanced fluctuations in the feedback signal, the feedback circuit being used to keep the current through the single-electron transistor constant by controlling its voltage relative to the 2D electron system.

With respect to the preceding subsections, insignificance of edge channel effects in transport experiments is verified in a usual way by coincidence of the results obtained in Hall bar and Corbino geometries.

### D. True zero-field metal-insulator transition, phase boundary in parallel magnetic fields

As has been discussed above, the existence of extended states in quantizing magnetic fields is established by two independent experimental methods: (i) quantization of $\sigma_{xy}$; and (ii) vanishing activation energy and vanishing nonlinearity of current-voltage characteristics as extrapolated from the insulating phase. Theory is generally in agreement with this even though there are unresolved problems with finite bandwidth of the extended states in the Landau levels. In contrast, no extended states are expected in zero magnetic field, at least, for weakly-interacting 2D electron systems. The second experimental criterion, however, results in an opposite conclusion although it does not have absolute credibility alone. To sort it out, further support by independent experimental verifications is needed.

Another criterion is based on analysis of the temperature dependences of the resistivity in $B = 0$. Pro-

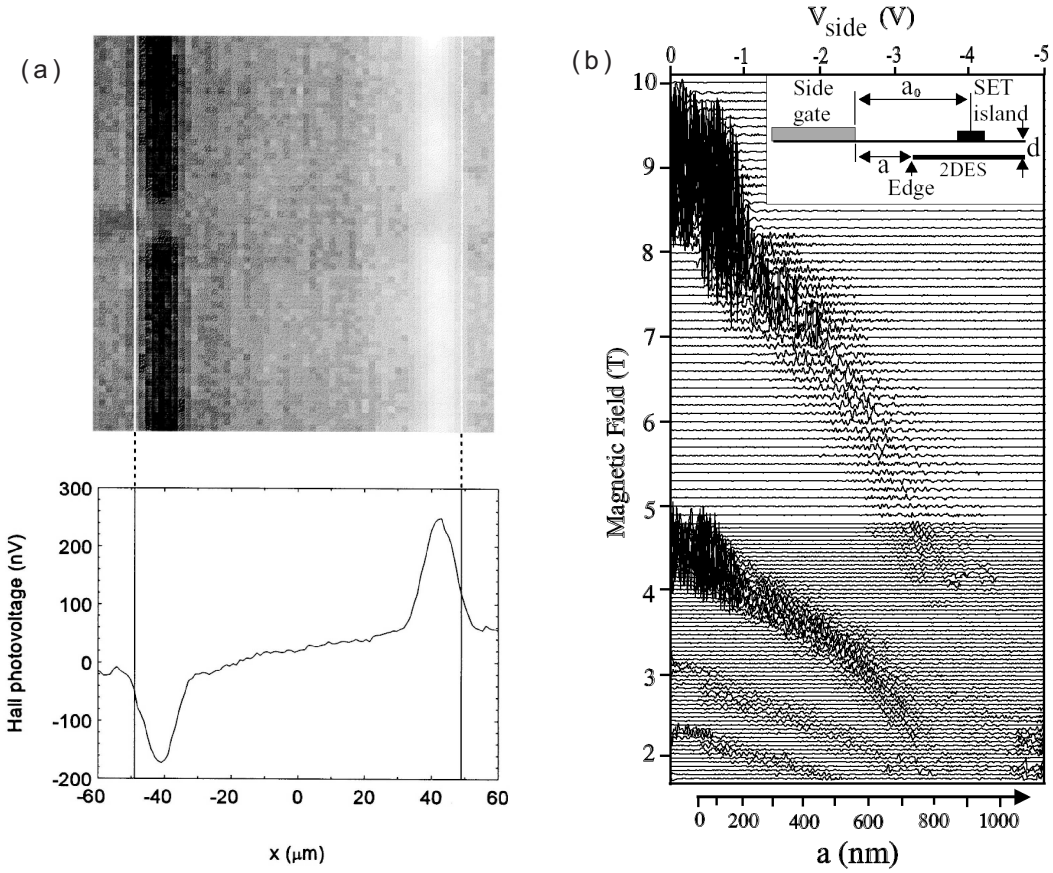


FIG. 11: (a) Image of the Hall photovoltage in a near surface GaAs/AlGaAs heterojunction at $\nu = 2$ (top) and a line scan taken horizontally through the image (bottom). The spot size is 5 $\mu$m across. The physical edges of the sample are indicated by vertical lines. From Ref. [183]. (b) Traces of the fluctuation part of the feedback signal vs the side-gate voltage for shifting the edge in a GaAs/AlGaAs heterostructure at different magnetic fields. Enhanced fluctuations in the feedback signal indicate vanishing $\sigma_{xx}$, which corresponds to Hall current channels (incompressible strips) for $\nu = 1$, 2, 3, and 4. Adopted from Ref. [184].

vided these are strong, those with positive (negative) derivative $d\rho/dT$ are indicative of a metal (insulator) [19, 20, 21, 75, 76]; note that in the vicinity of the transition, $\rho(T)$ dependences obey the scaling law with exponent $\kappa \approx 1$, which is consistent with the concept of thermal broadening/shift by the value $\sim k_B T$ of the effective mobility edge in the insulating phase (see section II B). If extrapolation of $\rho(T)$ to $T = 0$ is valid, the critical point for the metal-insulator transition is given by $d\rho/dT = 0$. In a low-disordered 2D electron system in silicon MOSFETs, the resistivity at a certain electron density shows virtually no temperature dependence over a wide range of temperatures [200, 201, 202] (see Fig. 12(a)). This curve separates those with positive and negative $d\rho/dT$ nearly symmetrically at temperatures above 0.2 K [203]. Assuming that it remains flat down to $T = 0$, one obtains the critical point $n_c$ which corresponds to a resistivity $\rho \approx 3h/e^2$ [31].

Recently, these two criteria have been applied simultaneously to the 2D metal-insulator transition in low-disordered silicon MOSFETs [77, 202]. In zero magnetic field, both methods yield the same critical density (see Figs. 12(b) and 13(b)). Since one of the methods is temperature independent, this equivalence strongly supports the existence of a true metal-insulator transition in $B = 0$. This also adds confidence that the curve with zero derivative $d\rho/dT$ will remain flat (or at least will retain finite resistivity value) down to zero temperature. Additional confirmation in favor of true zero-field metal-insulator transition is provided by magnetic measurements as described in the next section.

In the presence of a parallel magnetic field, $B_\parallel$, the outcome is very different. With increasing parallel field the transition point, $n_c(B_\parallel)$, determined from the vanishing nonlinearity and activation energy, shifts approximately linearly to higher electron densities, saturating above a critical field, $B_c \approx 3$ T, at a constant value which is approximately 1.5 times higher than that in zero field. Note that a similar suppression of the metallic state was observed using a cutoff criterion, $\rho = 100$ kOhm [108]. In

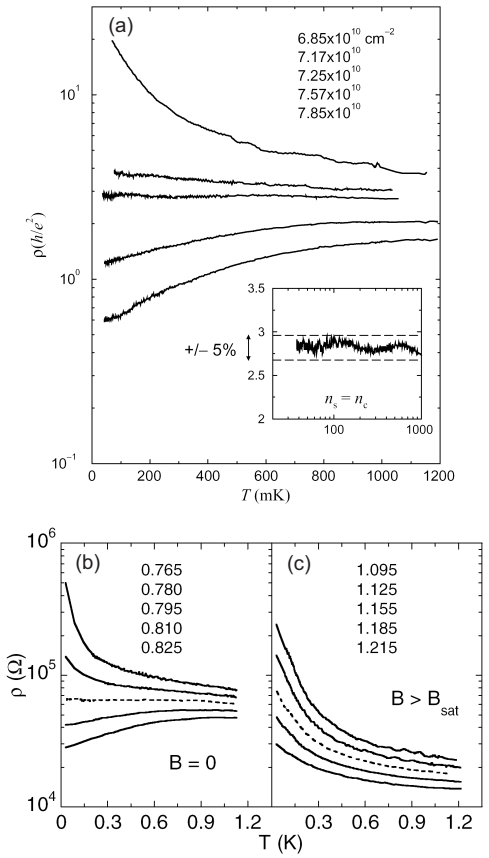


FIG. 12: (a) Resistivity as a function of temperature at different electron densities in a low-disordered silicon MOSFET. The inset shows the middle curve on an expanded scale. Adopted from Ref. [201]. (b, c) Temperature dependence of the resistivity of a low-disordered silicon MOSFET at different electron densities near the metal-insulator transition in zero magnetic field (b) and in a parallel magnetic field of 4 T (c). The electron densities are indicated in units of $10^{11}$ cm$^{-2}$. From Ref. [77].

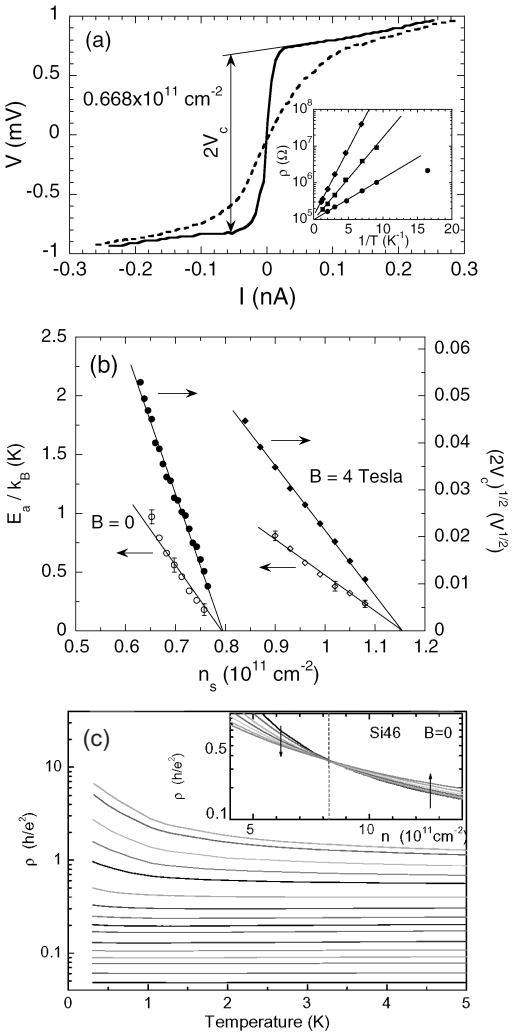


FIG. 13: (a) Current-voltage characteristics in zero magnetic field at $\approx 30$ (solid line) and 211 mK (dashed line) for the same silicon MOSFET as in Fig. 12(b, c); note that the threshold voltage is practically independent of temperature. An Arrhenius plot of the resistivity in the insulating phase is displayed in the inset for different values of $B_\parallel$ and $n_s$. From Ref. [77]. (b) Activation energy and square root of the threshold voltage as a function of electron density in zero magnetic field (circles) and in a parallel magnetic field of 4 T (diamonds). The critical densities correspond to the dashed lines in Fig. 12(b, c). From Ref. [77]. (c) Resistivity versus temperature in a strongly-disordered silicon MOSFET at the following electron densities: 3.85, 4.13, 4.83, 5.53, 6.23, 7.63, 9.03, 10.4, 11.8, 13.2, 16.0, 18.8, 21.6, 24.4, 30.0, and $37.0 \times 10^{11}$ cm$^{-2}$. The $\rho(n_s)$ isotherms are shown in the inset. Adopted from Ref. [85].

the metallic phase the saturation of the resistance with parallel field signals the onset of full spin polarization of the 2D electrons, as inferred from an analysis of the Shubnikov-de Haas oscillations in tilted magnetic fields [204, 205, 206]. One expects that the 2D electron system is spin polarized at parallel fields $B_\parallel > B_c$, and that the observed phase boundary shift is a spin effect. At the so-determined critical density $n_c(B_\parallel)$, the exponential divergence of the resistivity as $T \to 0$ ends, although $d\rho/dT$ remains negative at least for $B_\parallel > B_c$ (see Figs. 12(c) and 13(b)). In sharp contrast with the zero-field case, not only are the $\rho(T)$ curves in the field nonsymmetric about the middle curve in Fig. 12(c), but all of them have negative derivatives $d\rho/dT$ in the entire temperature range, although the values of $\rho$ are comparable to those in the $B = 0$ case. The metallic ($d\rho/dT > 0$) temperature dependence of the resistivity, observed at higher electron densities in parallel magnetic fields, is weak so that the derivative method does not yield a critical density at $B_\parallel > B_c$. Its failure leaves uncertain the existence of a true metal-insulator transition in a parallel magnetic field.

A very similar conclusion holds for 2D electron systems with higher disorder in zero magnetic field (see sec-

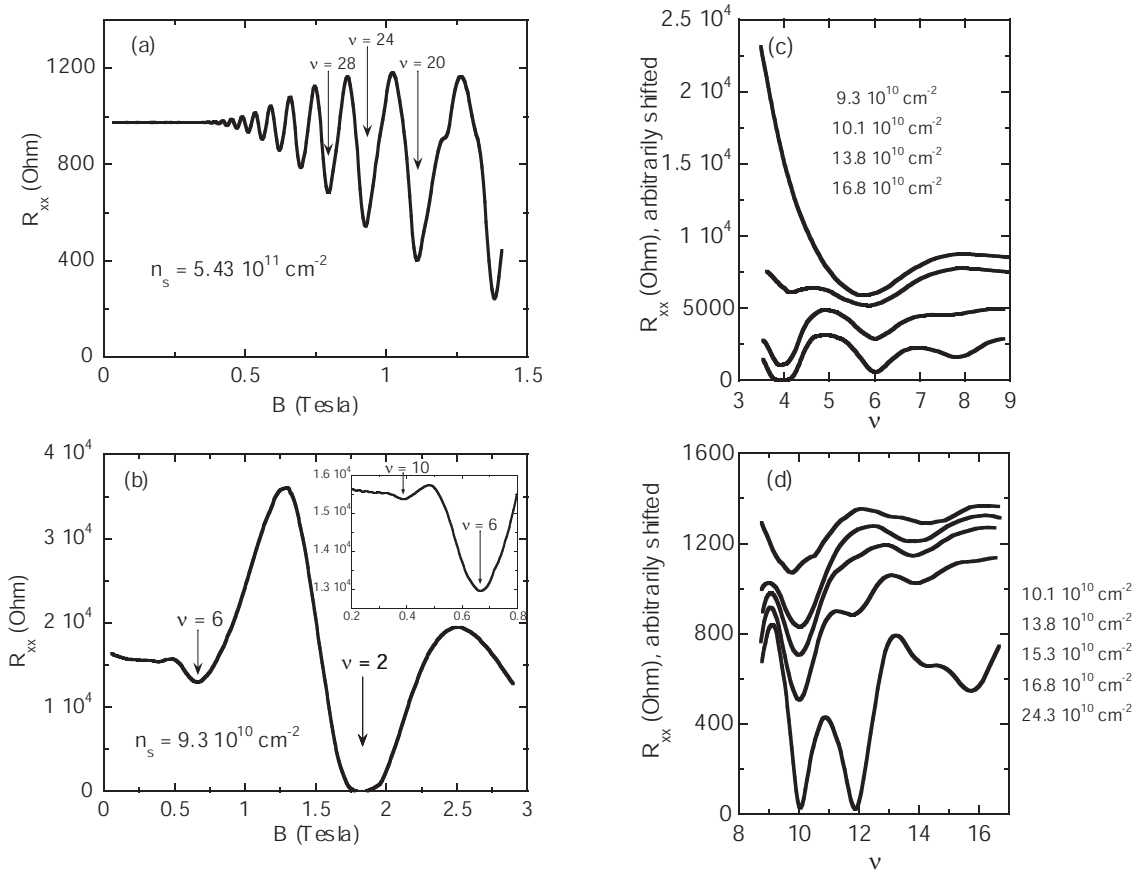


FIG. 14: Shubnikov-de Haas oscillations in a low-disordered silicon MOSFET at a temperature $\approx 40$ mK for high (a) and low (b) electron densities. (c, d) Evolution of the Shubnikov-de Haas oscillations with electron density in two ranges of filling factors. The curves are arbitrarily shifted along the $y$-axis for clarity. From Ref. [22].

tion II A). In this case the metallic ($d\rho/dT > 0$) behavior is also suppressed [78, 79, 80, 81, 82, 83, 84, 85] or disappears entirely, and extrapolation of the weak $\rho(T)$ dependences to $T = 0$ is not justified invalidating the derivative criterion for the critical point for the metal-insulator transition (see Fig. 13(c)). This is noteworthy that owing to its simplicity, the derivative method is widely used for describing metallic ($d\rho/dT > 0$) and insulating ($d\rho/dT < 0$) temperature dependences of resistance in a restricted temperature range. To avoid confusion with metallic and insulating phases, however, one should employ alternative methods for determining the metal-insulator transition point. Such methods including a vanishing activation energy and noise measurements have been applied to highly-disordered 2D carrier systems [202, 207, 208]. Being similar, they yield lower critical densities for the metal-insulator transition compared to those obtained using formally the derivative criterion. This simply reflects the fact that the metallic ($d\rho/dT > 0$) behavior is suppressed, the critical density $n_c$ increasing naturally with disorder strength (see Fig. 1).

## III. MANY-BODY PHENOMENA IN DILUTE 2D ELECTRON SYSTEMS

The resistivity drop with decreasing temperature in a low-disordered 2D electron system in silicon MOSFETs in zero magnetic field being strong compared to the metallic $\rho(T)$ expected from the temperature-dependent screening theories [209, 210, 211, 212], it was attributed to a manifestation of strong electron-electron interactions [19]. Recently, the underlying physics of the effect has been clarified. At low electron densities, a strongly enhanced ratio $gm$ of the spin and the cyclotron splittings has been found indicating that the 2D system behaves well beyond the weakly interacting Fermi liquid [22]. Experimental results have also shown that it is the effective mass that increases sharply at low electron densities and is related to the anomalous rise of the resistivity with temperature [28]. In view of $T = 0$ quantum phase transitions, while for the insulating phase a transition is signaled by the diverging localization length, the interaction-enhanced mass may be a similar indicator for the metallic phase.

### A. Strong increase of the product $gm$ near the metal-insulator transition, possible ferromagnetic transition

#### 1. Beating pattern of Shubnikov-de Haas oscillations

Electron-electron interactions give rise to a renormalization of the Fermi-liquid parameters including the effective mass and $g$ factor [3]. Tracing Shubnikov-de Haas oscillation minima in a 2D electron system in tilted magnetic fields, it is easy to determine the ratio $gm$ of spin and cyclotron splittings which is proportional to the spin susceptibility $\chi$. In the range of high electron densities $\geq 2 \times 10^{11}$ cm$^{-2}$ in silicon MOSFETs, moderate enhancements of $gm$ by a factor of $\leq 2.5$ were observed [204, 213, 214], which is consistent with the concept of weakly interacting Fermi liquid.

At low electron densities in low-disordered silicon MOSFETs in perpendicular magnetic fields, the Shubnikov-de Haas oscillation minima corresponding to the cyclotron splittings ($\nu = 4$, 8, 12, 16,...) were found to disappear as the electron density is reduced [22] (see Fig. 14). Disregarding the minimum for the valley splitting at $\nu = 1$, only minima corresponding to the spin splittings ($\nu = 2$, 6, 10, 14,...) remain close to the metal-insulator transition which occurs in the studied samples at $n_c \approx 8 \times 10^{10}$ cm$^{-2}$. These results show that as one approaches the metal-insulator transition, the cyclotron gaps (which are equal to the difference between the cyclotron and spin splittings, ignoring the valley splitting) become smaller than the spin gaps and eventually vanish. The condition for vanishing is coincidence of the spin and the cyclotron splittings, or $gm/2m_e = 1$ (where $m_e$ is the free electron mass), which is higher by more than a factor of 5 than the value of this ratio in bulk silicon, $gm/2m_e = 0.19$. The effect cannot be explained in the framework of the many-body enhancement of spin gaps in a perpendicular magnetic field [215, 216, 217, 218, 219] because the disappearance of the cyclotron gaps in a wide range of magnetic fields would require an enhanced $g$ factor which is independent of magnetic field. This implies that the product $gm$ is nearly field-independent and approximately equal to its many-body enhanced zero-field value (see section III B). Thus, the spin susceptibility $\chi \propto gm$ is strongly enhanced near the metal-insulator transition.

Similar experiments in tilted magnetic fields cannot provide high accuracy in determining the behavior of the renormalized $gm$ at low electron densities because there are too few Shubnikov-de Haas oscillations near the metal-insulator transition. High accuracy was attained in experiments on the parallel-field magnetotransport.

#### 2. Scaling the parallel-field magnetoresistance and other methods

As the thickness of the 2D electron system in silicon MOSFETs is small compared to the magnetic length in accessible fields, the parallel magnetic field couples largely to the electrons' spins while the orbital effects are suppressed. The resistance in dilute silicon MOSFETs was found to be isotropic with respect to in-plane magnetic field and rise steeply with the field saturating to a constant value above a critical field $B_c$ which depends on electron density [220, 221, 222] (see Fig. 15(a)). As has been mentioned in section II D, the saturation field $B_c$ corresponds to the onset of full spin polarization of the electron system [204, 205, 206].

In a low-disordered 2D electron system in silicon MOSFETs, it was found that the normalized magnetoresistance, measured at different electron densities in the low-temperature limit in which $\rho(B_\parallel)$ becomes temperature independent, collapses onto a single curve when plotted as a function of $B_\parallel/B_c$, where the scaling parameter $B_c$ is normalized to correspond to the saturation/polarization field [23] (see Fig. 15(b, c)). The scaling breaks down when one approaches the metal-insulator transition where the magnetoresistance depends strongly on temperature even at the lowest experimentally achievable temperatures. Note that the observed scaling dependence is described reasonably well by the theoretical dependence of $\rho/\rho(0)$ on the degree of spin polarization, $\xi = gm\mu_B B_\parallel/\pi\hbar^2 n_s = B_\parallel/B_c$, based on the spin-polarization-dependent screening of a random potential [223]. The field $B_c$ is proportional, with high precision, to the deviation of the electron density from its critical value: $B_c \propto (n_s - n_c)$ (see Fig. 16(a)). The procedure used provides high accuracy for determining the functional form of $B_c(n_s)$, even though the absolute value of $B_c$ is determined not so accurately. Since the strong increase of the product $gm$ at low electron densities (see Fig. 16(b)), which follows from the $B_c(n_s)$ dependence, is in agreement with the enhanced $gm$ obtained by Shubnikov-de Haas oscillations, the band tail of localized electron states is small and the clean limit occurs. Therefore, the tendency for $B_c$ to vanish at a finite electron density $n_\chi$ close to $n_c$ gives evidence in favor of the existence of a ferromagnetic transition in this electron system indicating that the metal-insulator transition is driven by interactions [23]. It signifies that on the phase diagram of Fig. 1, the vicinity of either tricritical point is reached (see section III C).

A similar conclusion about possible spontaneous spin polarization was drawn based on a scaling of magnetoconductivity data in similar samples at different electron densities and temperatures [24]. Results for the strongly enhanced $gm$ were corroborated in detailed studies of Shubnikov-de Haas oscillations in dilute silicon MOSFETs with higher disorder in tilted magnetic fields [224] (see Fig. 16(c)). The agreement between all three sets of data is remarkable, especially if one takes into ac-

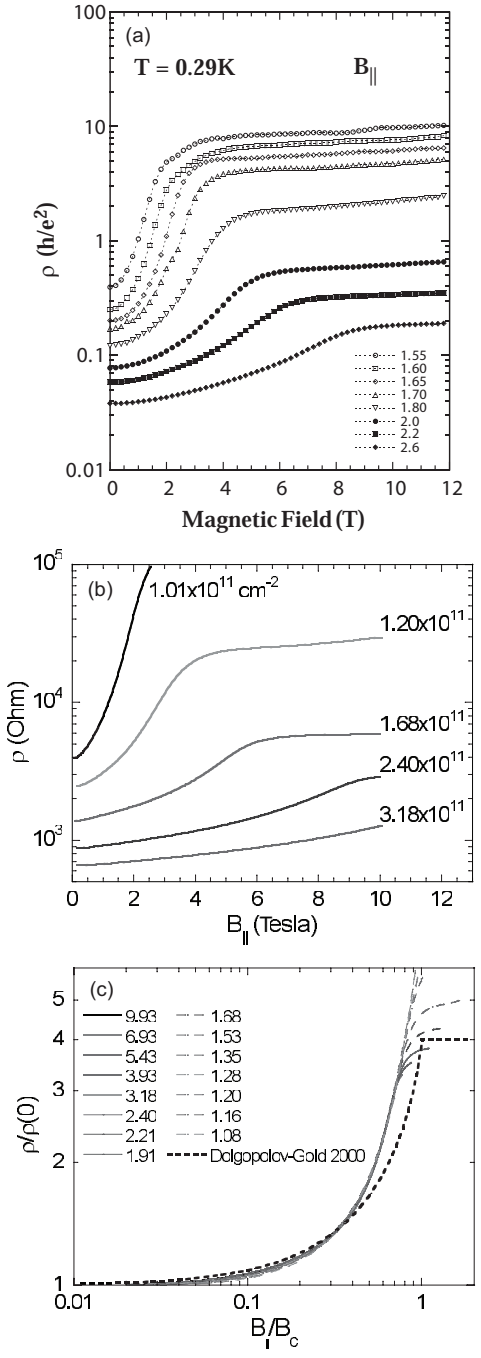


FIG. 15: (a) Resistivity versus parallel magnetic field measured on a low-disordered silicon MOSFET. Different symbols correspond to gate voltages from 1.55 to 2.6 V, or to densities from 1.01 to $2.17 \times 10^{11}$ cm$^{-2}$. Adopted from Ref. [221]. (b) Low-temperature magnetoresistance of a low-disordered 2D electron system in silicon MOSFETs in parallel magnetic fields at different densities above $n_c$ for the $B = 0$ metal-insulator transition. From Ref. [23]. (c) Scaled curves of the normalized magnetoresistance vs $B_\parallel/B_c$. The electron densities are indicated in units of $10^{11}$ cm$^{-2}$. Also shown by a dashed line is the normalized magnetoresistance calculated by Dolgopolov and Gold [223]. From Ref. [23].

count that different groups used different methods, different samples, and different field/spin-polarization ranges [25]. This also indicates that the electron density $n_\chi \approx 8 \times 10^{10}$ cm$^{-2}$ is sample independent, in contrast to the critical density $n_c$ for the metal-insulator transition. Obviously, for the spin susceptibility $\chi \propto gm$ to diverge at $n_s = n_\chi$, the extrapolation of $B_c(n_s)$ to zero must be valid. To verify its validity, accurate data at lower densities, lower temperatures, and on much less disordered samples are needed [25, 225, 226].

Thermodynamic investigations of the spin susceptibility, based on measurements of the chemical potential change with parallel magnetic field, $d\mu/dB_\parallel$, were performed in highly-disordered silicon MOSFETs, as inferred from the considerably higher densities for the metal-insulator transition [227] (see Fig. 16(d), cf. Fig. 16(c)). As compared to the clean regime, the obtained dependence of the polarization field $B_c$ on $n_s$ in Fig. 16(d) is shifted to appreciably higher electron densities caused by local moments in the band tail [222, 227, 228, 229]. The band tail effects thus become crucial in parallel-field experiments on highly-disordered 2D electron systems.

### *3. Other 2D carrier systems*

In dilute GaAs/AlGaAs heterostructures, a similar enhancement of the spin susceptibility at low electron densities was found by an analysis of the Shubnikov-de Haas oscillations [27] (see Fig. 17(a)). The thickness of the 2D carrier system in GaAs/AlGaAs heterostructures is relatively large, which leads to an increase of the effective mass with parallel magnetic field [27, 230, 231, 232, 233, 234]. As a result, the value of polarization field obtained from the parallel-field magnetoresistance becomes strongly reduced as the electron density increases. Disregarding this reduction, both data sets determine the $B_c(n_s)$ dependence whose critical behavior is not so evident, possibly because the lowest experimentally reached densities are still too high. Due to the lower effective mass, higher dielectric constant, and the absence of valley degeneracy, the same interaction strength $r_s^* = E_{ee}/E_F$ in the 2D electron system in GaAs/AlGaAs heterostructures is expected to be achieved at densities about two orders of magnitude lower than in silicon MOSFETs. Therefore, the critical region is expected at densities $n_s < 10^9$ cm$^{-2}$ which have not yet been accessed in currently available samples of GaAs/AlGaAs heterostructures.

The orbital effects in parallel magnetic fields can be avoided by using narrow quantum wells. A 2D electron system in narrow AlAs quantum wells is similar to that in silicon MOSFETs, except that in the former the valley degeneracy is absent [235]. The critical region expected at densities $n_s < 2 \times 10^{10}$ cm$^{-2}$ is exceeded strongly by the lowest accessible electron densities in narrow AlAs quantum wells with high disorder (see Fig. 17(b)). Note

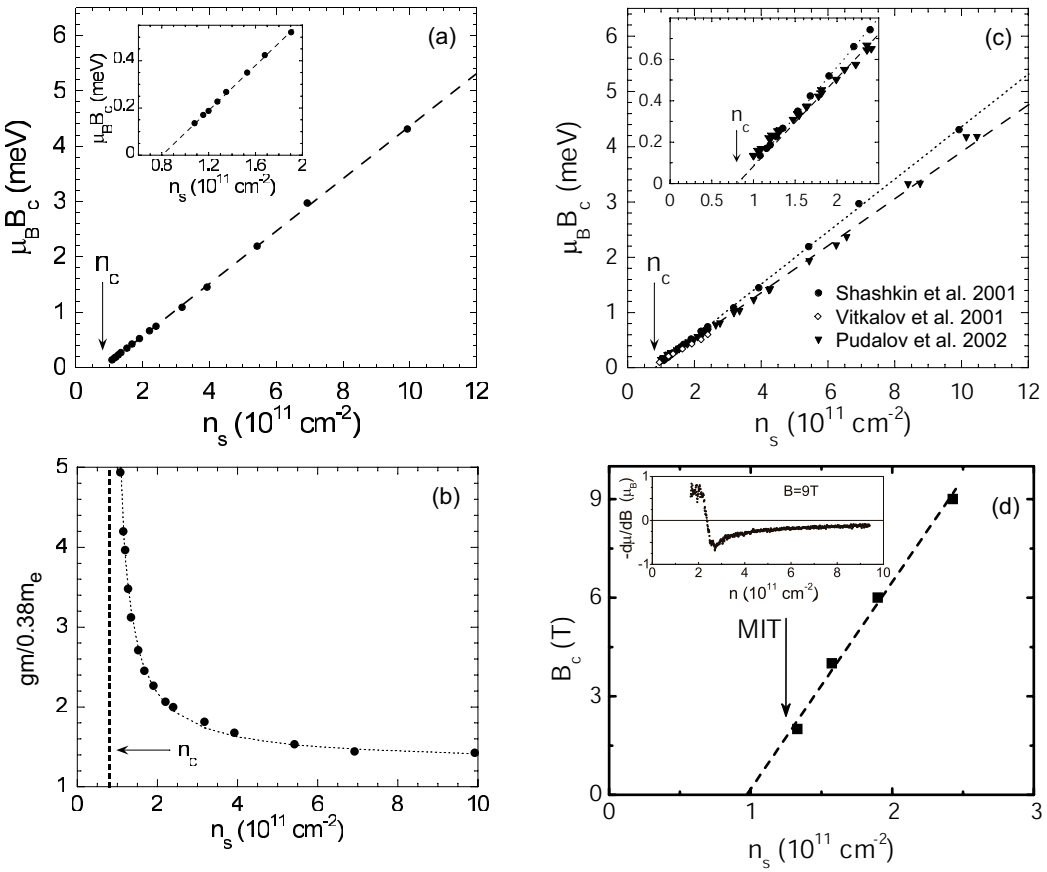


FIG. 16: (a) Dependence of the field $B_c$ on electron density in a low-disordered silicon MOSFET. The dashed line is a linear fit. From Ref. [23]. (b) The product $gm$ versus electron density obtained from the data for $B_c$. From Ref. [23]. (c) Polarization field as a function of electron density obtained by different groups [23, 24, 224]. The critical density $n_c$ in the samples of Ref. [23] is indicated. From Ref. [25]. (d) Polarization field vs electron density in a highly-disordered silicon MOSFET as determined from $d\mu/dB_\parallel = 0$ at 0.2 K. The dashed line is a linear fit. The evaluated position of the metal-insulator transition is indicated. The derivative $d\mu/dB_\parallel$ as a function of electron density in a parallel magnetic field of 9 T at a temperature of 100 mK is displayed in the inset. Adopted from Ref. [227].

that the data points in the insulating phase reflect the physics of local moments in the band tail [222, 227, 228, 229], which is different from that of the metallic phase.

Being very similar to silicon MOSFETs, a 2D electron system in Si/SiGe quantum wells is different by the higher dielectric constant and the presence of a spacer. Moreover, it is distinguished from other systems by its remote-doping scattering as indicated by the small parallel-field magnetoresistance [236]. A similar increase of the spin susceptibility at low densities was observed in this electron system, the lowest achievable densities also being well above the expected critical region at $n_s < 4 \times 10^{10}$ cm$^{-2}$ [237]. So, in all the studied dilute 2D electron systems other than silicon MOSFETs, too high disorder and, hence, too high densities for the metal-insulator transition (see Fig. 1) mask possible critical behavior of the spin susceptibility.

## B. Determining separately the effective mass and $g$ factor

### 1. *Slope of the metallic temperature dependence of conductivity in zero magnetic field*

The strong enhancement of the spin susceptibility $\chi \propto gm$ at low electron densities can be caused in principle by an increase of either $g$ or $m$ or both. The effective mass and $g$ factor were determined separately using the recent theory of temperature-dependent corrections to conductivity due to electron-electron interactions [238]. Note that its main advantage compared to the temperature-dependent screening theories [209, 210, 211, 212] is that spin exchange effects are treated carefully in the new theory. At intermediate temperatures, the predicted $\sigma(T)$ is a linear function

$$\frac{\sigma(T)}{\sigma_0} = 1 - A^* k_B T, \qquad A^* = -\frac{(1+8F_0^a)gm}{\pi\hbar^2 n_s}, \quad (5)$$

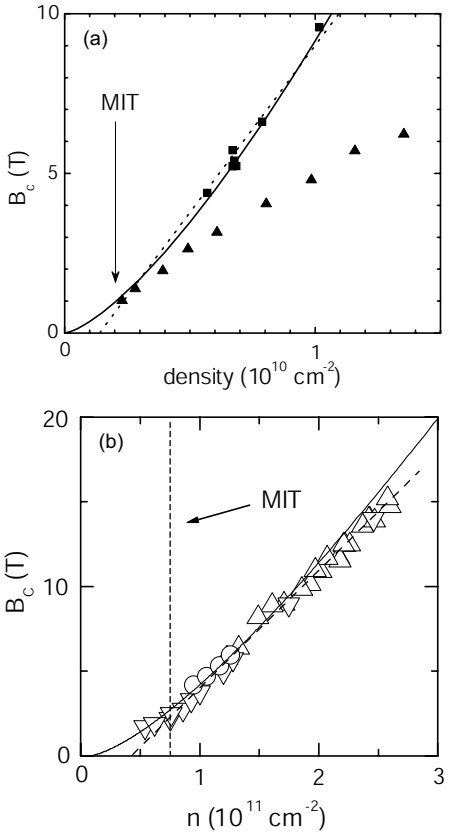


FIG. 17: (a) Data for $B_c$ as a function of electron density in a dilute GaAs/AlGaAs heterostructure obtained by Shubnikov-de Haas oscillations (squares) and parallel-field magnetoresistance (triangles). The power-law fit $B_c \propto n_s^{1.4}$ (solid line) is compared to the linear fit (dashed line). Also shown is the evaluated position of the metal-insulator transition. Adopted from Ref. [27]. (b) Dependence of $B_c$ on electron density obtained by measurements of the parallel-field magnetoresistance in highly-disordered samples of narrow AlAs quantum wells. The solid curve represents the quantum Monte Carlo calculation for a disorder-free 2D electron system [5]. The dashed line is a linear fit. The evaluated position of the metal-insulator transition is indicated. Adopted from Ref. [235].

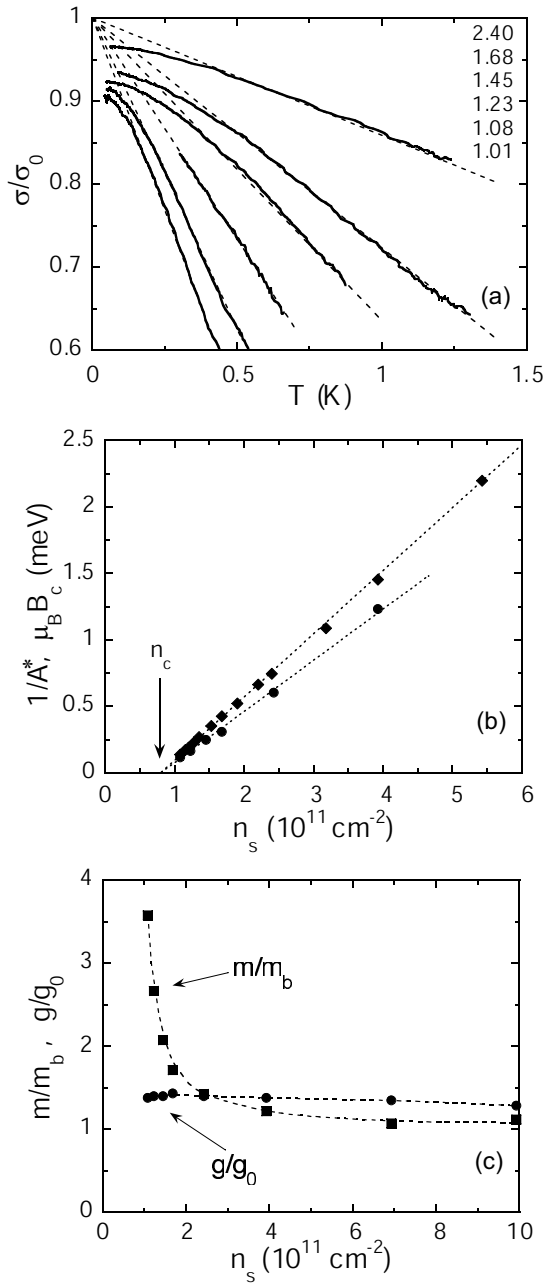


FIG. 18: (a) The temperature dependence of the normalized conductivity at different electron densities (indicated in units of $10^{11}$ cm$^{-2}$) in a low-disordered silicon MOSFET above the critical electron density for the metal-insulator transition. The dashed lines are fits to the linear interval of the dependence. (b) The inverse slope $1/A^*$ (circles) and the polarization field $B_c$ (diamonds) as a function of electron density. The dashed lines are linear fits which extrapolate to the critical density for the metal-insulator transition. (c) The effective mass and $g$ factor versus electron density determined from an analysis of the temperature-dependent conductivity and parallel-field magnetoresistance. The dashed lines are guides to the eye. From Ref. [28].

where $\sigma_0$ is the value obtained by extrapolating the linear interval of the $\sigma(T)$ dependence to $T = 0$ and the factor of 8 is expected for temperatures lower than the valley splitting in silicon MOSFETs. The slope, $A^*$, is determined by the Fermi liquid constants $F_0^a$ and $F_1^s$ that define the renormalization of $g$ and $m$: $g/g_0 = 1/(1+F_0^a)$ and $m/m_b = 1 + F_1^s$. Using these relations one obtains both $g$ and $m$ from the data for the slope $A^*$ and the product $gm$ [28].

For sufficiently small deviations $|\sigma/\sigma_0 - 1|$, the dependence of the normalized conductivity $\sigma/\sigma_0$ on temperature at different electron densities above the critical density $n_c$ for the metal-insulator transition is linear over a wide enough interval of temperatures (see Fig. 18(a)). The inverse slope $1/A^*$ and the value $\mu_B B_c$ are close to each other in a wide range of electron densities (see

Fig. 18(b)). Moreover, the low density data for $1/A^*$ are approximated well by a linear dependence which extrapolates to the critical density $n_c$ in a way similar to the behavior of $B_c$. This finding immediately points to approximate constancy of the $g$ factor at low electron densities, according to the functional form of the slope $A^*$ in Eq. (5).

Renormalizations $g/g_0$ and $m/m_b$ versus electron density determined from this analysis corroborate earlier results at high densities but are striking in the limit of low electron densities (see Fig. 18(c)). In the high $n_s$ region, the enhancement of both $g$ and $m$ is relatively small, both values increasing slightly with decreasing electron density in agreement with earlier data [239]. Also, the renormalization of the $g$ factor is dominant compared to that of the effective mass, consistent with theoretical studies [240, 241, 242]. In contrast, in the low $n_s$ region, the renormalization of the effective mass increases sharply with decreasing density while the $g$ factor remains nearly constant. Hence, it is the effective mass, rather than the $g$ factor, that is responsible for the drastically enhanced spin susceptibility near the metal-insulator transition.

Normally, no difference is assumed between the interaction parameter $r_s^* = E_{ee}/E_F$ and the Wigner-Seitz radius $r_s = 1/(\pi n_s)^{1/2} a_B$. The finding of the strongly enhanced effective mass breaks the equivalence of $r_s^*$ and $r_s$ because they are connected through the $n_s$ dependent mass: $r_s^* = 2(m/m_b)r_s$ (where the factor of 2 comes from the valley degeneracy in silicon MOSFETs). Therefore, as one approaches the metal-insulator transition in low-disordered silicon MOSFETs, the interaction parameter $r_s^*$ grows much more rapidly than $r_s$ reaching the values $r_s^* > 50$ [28].

In similar experimental verifications of the theory [238] on different 2D carrier systems, much higher values $F_0^a$ than the expected limit $F_0^a = -1$ for the Stoner instability were found for the metallic slope of $\sigma(T)$ [243, 244, 245, 246]. The relatively small enhancement of the $g$ factor indicates that the spin exchange effects are not very pronounced. From an experimental point of view, this raises a problem of comparison between different theories. Formally, even if there are possible uncertainties in the theoretical coefficients, both the temperature-dependent screening theories [209, 210, 211, 212] and the theory [238] describe reasonably well available experimental data [247, 248]. To discriminate between these two, more detailed comparison with experiment is needed. Note that in all theories, the slope $A^*$ in Eq. (5) is proportional to the effective mass, so the conclusion about the strongly enhanced effective mass at low electron densities in low-disordered silicon MOSFETs is basically independent of a particular theory.

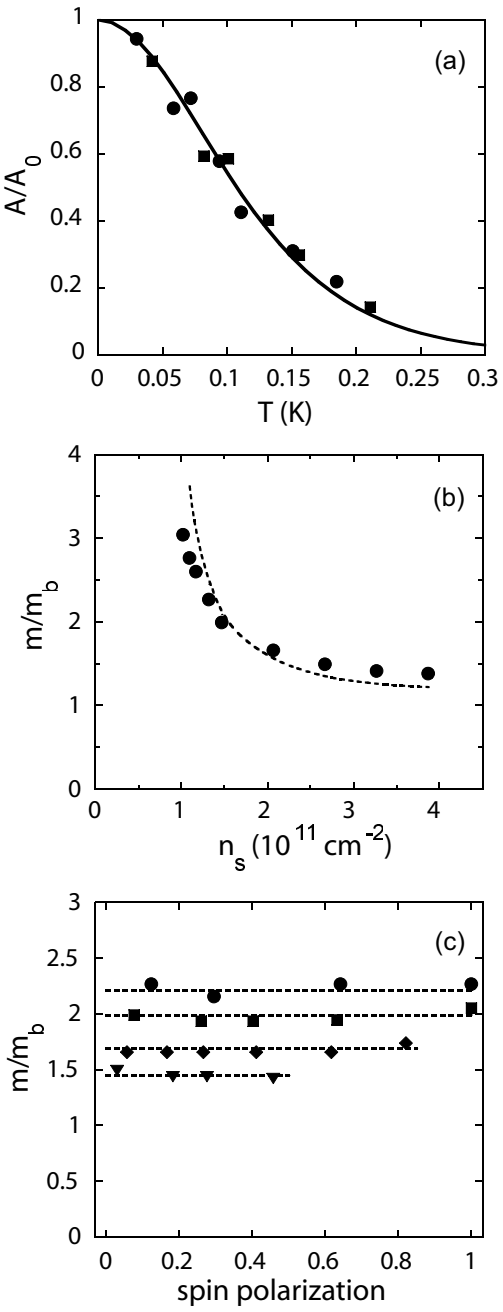


FIG. 19: (a) Change of the amplitude of the weak-field Shubnikov-de Haas oscillations in a low-disordered silicon MOSFET with temperature at $n_s = 1.17 \times 10^{11}$ cm$^{-2}$ for oscillation numbers $\nu = 10$ (circles) and $\nu = 14$ (squares). The value of $T$ for the $\nu = 10$ data is divided by the factor of 1.4. The solid line is a fit using Eq. (6). (b) Dependence of the effective mass on electron density determined from an analysis of Shubnikov-de Haas oscillations (circles) and from an analysis of $\sigma(T)$ and $\rho(B_\parallel)$ (dashed line). (c) The effective mass versus the degree of spin polarization for the following electron densities in units of $10^{11}$ cm$^{-2}$: 1.32 (circles), 1.47 (squares), 2.07 (diamonds), and 2.67 (triangles). The dashed lines are guides to the eye. From Ref. [29].

### 2. Temperature dependent amplitude of the weak-field Shubnikov-de Haas oscillations

The claim about the strong increase of the effective mass was verified based on analysis of the temperature dependence of the Shubnikov-de Haas oscillations. The method is similar to that used by Smith and Stiles [214] but is extended to much lower electron densities and temperatures [29]. In the low temperature limit, the $\rho(T)$ dependence saturates, and the Lifshitz-Kosevich formula with constant Dingle temperature for the weak-field oscillation amplitude for the normalized resistance

$$\frac{A(T)}{A_0} = \frac{2\pi^2 k_B T/\hbar\omega_c}{\sinh(2\pi^2 k_B T/\hbar\omega_c)}, \qquad A_0 = 4\exp(-2\pi^2 k_B T_D/\hbar\omega_c) \tag{6}$$

(where $\omega_c = eB_\perp/mc$ is the cyclotron frequency and $T_D$ is the Dingle temperature) describes damping of the Shubnikov-de Haas oscillations with temperature (see Fig. 19(a)). The effective mass as a function of electron density determined by this method agrees well with the data obtained by the procedure described in the preceding section (see Fig. 19(b)). The agreement between the results obtained using two independent methods supports the validity of both and justifies applicability of Eq. (6) to the strongly interacting 2D electron system in silicon MOSFETs.

To probe a possible contribution from the spin exchange effects to the effective mass enhancement, a parallel magnetic field component was introduced to align the electrons' spins. Within the experimental accuracy, the effective mass does not depend on the degree of spin polarization $\xi = (B_\perp^2 + B_\parallel^2)^{1/2}/B_c$ (see Fig. 19(c)). Therefore, the $m(n_s)$ dependence is robust, and the origin of the mass enhancement has no relation to the electrons' spins and exchange effects.

A similar analysis of the Shubnikov-de Haas oscillations in dilute silicon MOSFETs at high temperatures $T > 0.3$ K, where the low-density resistivity (and, hence, $T_D$) depends strongly on temperature, allows an evaluation of the effective mass as well as the $g$ factor which is calculated from the known value of $gm$ [224] (see Fig. 20). The two data sets are obtained based on an assumption of a temperature-independent Dingle temperature and that of a Dingle temperature that increases linearly with temperature. Too large uncertainty of the results makes it impossible to establish which value (either $g$ or $m$ or both) is responsible for the strong enhancement of the spin susceptibility. Note that an attempt to improve the evaluation of the effective mass by justifying the application of the Lifshitz-Kosevich formula with temperature dependent $T_D$ [249] would lead on the contrary to bigger deviations of the estimated values of mass from the data obtained in the low temperature limit (cf. Figs. 19(b) and 20).

An analysis of the temperature dependent amplitude of Shubnikov-de Haas oscillations in a dilute 2D electron system in narrow AlAs quantum wells yielded moderate enhancements of the effective mass as well as the $g$ factor determined from the known $gm$ [235]. The observed behavior of $g$ and $m$ is similar to that found at high electron densities in silicon MOSFETs. This indicates that the valley origin of the strongly enhanced effective mass at low electron densities in silicon MOSFETs is not very likely, even though the lowest accessible densities in narrow AlAs quantum wells are still too high. Interestingly, the observed values of $g/g_0$ in the limit of high electron densities in AlAs quantum wells exceed appreciably the value of $g/g_0 = 1$ as well as those in silicon MOSFETs. The increase of the spin susceptibility with the strain-induced valley polarization, observed at high electron densities in AlAs quantum wells [250], is likely to be connected with the increase in the $g$ factor.

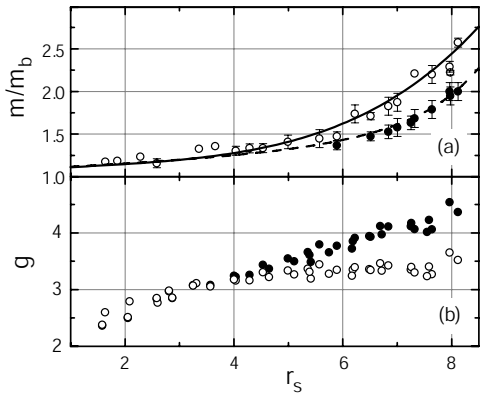


FIG. 20: The effective mass and $g$ factor in a dilute silicon MOSFET as a function of $r_s$. Different symbols correspond to two different assumptions for evaluating $m$ from an analysis of the high-temperature Shubnikov-de Haas oscillations: a temperature-independent $T_D$ (open circles) and a Dingle temperature that increases linearly with temperature (solid circles). The solid and dashed lines in (a) are polynomial fits. Adopted from Ref. [224].

### 3. Spin and cyclotron gaps in strong magnetic fields

The results for the strong enhancement of the effective mass are also consistent with the data for spin and cyclotron gaps obtained by magnetocapacitance spectroscopy. The method is based on determination of the chemical potential jumps in a 2D electron system when the filling factor traverses the gaps in the spectrum. A dip in the magnetocapacitance at integer filling factor is directly related to a jump of the chemical potential across a corresponding gap in the spectrum of the 2D electron system [251, 252]:

$$\frac{1}{C} = \frac{1}{C_0} + \frac{1}{A_g e^2 dn_s/d\mu}, \tag{7}$$

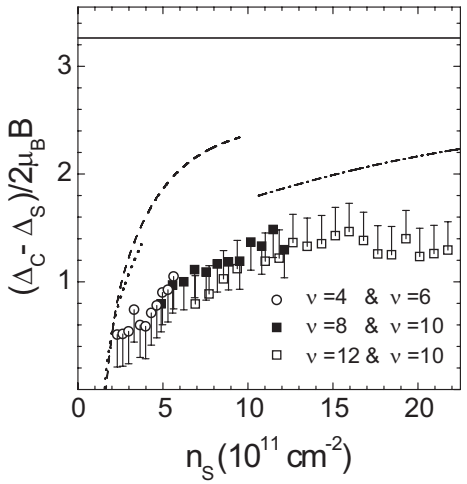


FIG. 21: For silicon MOSFETs, difference of the normalized values of cyclotron and spin gaps in a perpendicular magnetic field versus electron density. The level width contribution is indicated by systematic error bars. Also shown for comparison is the value $(m_e/m - g)$ determined from the data of Ref. [28] (dashed line), Ref. [29] (dotted line), and Ref. [214] (dash-dotted line) as well as using the band electron mass and the $g$ factor in bulk silicon (solid line). From Ref. [254].

where $C_0$ is the geometric capacitance and $A_g$ is the sample area. The chemical potential jump is determined by integrating the magnetocapacitance over the dip in the low temperature limit where the magnetocapacitance saturates and becomes independent of temperature [253]. Note that standard measurements of activation energy yield a mobility gap which may be different from the gap in the spectrum. This is a serious disadvantage as compared to the direct method of magnetocapacitance spectroscopy.

The $g$ factor determined by this method is close to its value in bulk silicon and does not change with the filling factor [254], in disagreement with the theory of exchange-enhanced gaps [215, 216, 217, 218, 219]. The cyclotron splitting corresponds to the effective mass that is strongly enhanced at low electron densities (see Fig. 21). Thus, in strong magnetic fields, the spin exchange effects are still not pronounced.

It is worth noting that in contrast to the $g$ factor, the valley gap is strongly enhanced at the lowest filling factors $\nu = 1$ and $\nu = 3$ and oscillates with $\nu$ [253, 254]. This is similar to the behavior of the spin gap in GaAs/AlGaAs heterostructures [255, 256], both of the gaps increasing linearly with perpendicular magnetic field.

### C. Wigner crystal or ferromagnetic Fermi liquid, theoretical approaches

As has been mentioned above, the experimental results obtained in low-disordered silicon MOSFETs indicate that on the metallic side the metal-insulator transition is driven by interactions. In contrast, on the insulating side this is still a classical percolation transition with no dramatic effects from interactions. One concludes that the vicinity of either tricritical point on the phase diagram in Fig. 1 is reached. This is consistent with the fact that the interaction parameter $r_s^*$ at low electron densities exceeds the theoretical estimate for the onset of Wigner crystallization, even though it is not yet clear whether or not electron crystallization expected in the low density limit is preceded by an intermediate phase like ferromagnetic Fermi liquid.

To face the problem, two approaches have been formulated. The first one exploits the Fermi liquid model extending it to relatively large $r_s^*$. Its outcome is that the renormalization of $g$ is large compared to that of $m$ [240, 241, 242]. In the limiting case of high $r_s^*$, one may expect a divergence of the $g$ factor that corresponds to the Stoner instability. These predictions are in contradiction to the experimental data. Firstly, the dilute system behavior in the regime of the strongly enhanced susceptibility — close to the onset of spontaneous spin polarization and Wigner crystallization — is governed by the effective mass, rather than the $g$ factor, through the interaction parameter $r_s^*$. And secondly, the insensitivity of the effective mass enhancement to spin exchange effects cannot be accounted for. This discrepancy reduces somewhat the chances for the occurrence of a ferromagnetic Fermi liquid that precedes electron crystallization. In principle, should the spin exchange be small, the spin effects may still come into play closer to the onset of Wigner crystallization where the Fermi energy may continue dropping as caused by mass enhancement.

The other theoretical approach is not based on Fermi liquid. In analogy with $He^3$, it was predicted the existence of an intermediate phase between the Fermi liquid and the Wigner crystal, caused by a partial separation of the uniform phases [257]. It was also predicted that near the crystallization point, the renormalization of $m$ is dominant compared to that of $g$ and that the effective mass may diverge at the transition and should increase with the magnetic field [258]. The strong increase of the effective mass near electron crystallization also follows from Gutzwiller's variational method [259], which was applied to silicon MOSFETs [260], and from the dynamical mean-field theory [261]. Although the sharp increase of the mass is in agreement with the experimental results, the suggested dependence of $m$ on the degree of spin polarization is not confirmed by the data.

Concluding this section, I would like to make some more remarks on the Fermi-liquid-related concepts. An idea was expressed to connect the observed effective mass enhancement to possible formation of a coupled-valley

state in bivalley electron systems [262, 263]. Still, it is at odds with the fact that similar results are obtained for single-valley electron systems. An assumption was made that a plateau at the Fermi energy in the spectrum $E(k)$ may form leading to a diverging effective mass (see, e.g., Ref. [264]). As for now, however, the dependence of the effective mass on temperature, resulting from the plateau formation, is not consistent with the experimental findings. A prediction that the electron density, at which the effective mass exhibits a sharp increase, is sensitive to disorder [265] is not confirmed by the experimental data in available samples. After all, one can simply follow a classical way of introducing phenomenologically Fermi-liquid parameters as the physical observables to be determined in experiment.

## IV. CONCLUSIONS

A critical analysis of the available experimental data for 2D electron systems shows that consequences of the scaling theory of localization are not confirmed. The main points to be addressed by theory are the problem of finite bandwidth of the extended states in the Landau levels, and that of a true metal-insulator transition in zero magnetic field whose existence is strongly supported in low-disordered 2D electron systems, but remains uncertain in 2D electron systems with high disorder. Also, there is still no theoretical description of the oscillations of the metal-insulator phase boundary as a function of perpendicular magnetic field.

In the past four years, significant progress was made in understanding the metallic state in strongly-interacting, low-disordered 2D electron systems. The state is remarkable by the strong metallic temperature dependence of the resistivity caused by electron-electron interaction effects. The spin susceptibility measured in low-disordered silicon MOSFETs using different experimental methods shows a sharp increase and possible divergence at a finite sample-independent electron density $n_\chi$ close to the critical density $n_c$ for the metal-insulator transition. This indicates that the metal-insulator transition in clean 2D systems is driven by interactions. Unlike the Stoner instability, the increase in the spin susceptibility is caused by the enhanced effective mass rather than the $g$ factor. The effective mass does not depend on the degree of spin polarization, so the mass enhancement is not due to spin exchange. A similar increase in the spin susceptibility is observed in other 2D carrier systems. It remains to be seen whether or not it indicates the occurrence of a spontaneous spin polarization at a finite carrier density.

I am grateful to I. L. Aleiner, M. W. C. Dharmawardana, V. T. Dolgopolov, M. M. Fogler, V. F. Gantmakher, D. Heiman, S. V. Kravchenko, D. N. Sheng, and A. Widom for valuable discussions. The author is supported by the Russian Foundation for Basic Research and Ministry of Education and Science.

[1] Wigner E *Phys. Rev.* **46** 1002 (1934)
[2] Stoner E C *Rep. Prog. Phys.* **11** 43 (1946)
[3] Landau L D *Sov. Phys. JETP* **3** 920 (1957)
[4] Tanatar B, Ceperley D M *Phys. Rev. B* **39** 5005 (1989)
[5] Attaccalite C, Moroni S, Gori-Giorgi P, Bachelet G B *Phys. Rev. Lett.* **88** 256601 (2002)
[6] Abrahams E, Anderson P W, Licciardello D C, Ramakrishnan T V *Phys. Rev. Lett.* **42** 673 (1979)
[7] Altshuler B L, Aronov A G, Lee P A *Phys. Rev. Lett.* **44** 1288 (1980)
[8] Finkelstein A M *Sov. Phys. JETP* **57** 97 (1983)
[9] Finkelstein A M *Z. Phys. B* **56** 189 (1984)
[10] Castellani C, Di Castro C, Lee P A, Ma M *Phys. Rev. B* **30** 527 (1984)
[11] Dolan G J, Osheroff D D *Phys. Rev. Lett.* **43** 721 (1979)
[12] Bishop D J, Tsui D C, Dynes R C *Phys. Rev. Lett.* **44** 1153 (1980)
[13] Uren M J, Davies R A, Pepper M *J. Phys. C* **13** L985 (1980)
[14] Shashkin A A, Kravchenko G V, Dolgopolov V T *JETP Lett.* **58** 220 (1993)
[15] Shashkin A A, Dolgopolov V T, Kravchenko G V *Phys. Rev. B* **49** 14486 (1994)
[16] Shashkin A A, Dolgopolov V T, Kravchenko G V, Wendel M, Schuster R, Kotthaus J P, Haug R J, von Klitzing K, Ploog K, Nickel H, Schlapp W *Phys. Rev. Lett.* **73** 3141 (1994)
[17] Khmelnitskii D E *Phys. Lett. A* **106** 182 (1984)
[18] Laughlin R B *Phys. Rev. Lett.* **52** 2304 (1984)
[19] Kravchenko S V, Kravchenko G V, Furneaux J E, Pudalov V M, D'Iorio M *Phys. Rev. B* **50** 8039 (1994)
[20] Kravchenko S V, Mason W E, Bowker G E, Furneaux J E, Pudalov V M, D'Iorio M *Phys. Rev. B* **51** 7038 (1995)
[21] Kravchenko S V, Simonian D, Sarachik M P, Mason W, Furneaux J E *Phys. Rev. Lett.* **77** 4938 (1996)
[22] Kravchenko S V, Shashkin A A, Bloore D A, Klapwijk T M *Solid State Commun.* **116** 495 (2000)
[23] Shashkin A A, Kravchenko S V, Dolgopolov V T, Klapwijk T M *Phys. Rev. Lett.* **87** 086801 (2001)
[24] Vitkalov S A, Zheng H, Mertes K M, Sarachik M P, Klapwijk T M *Phys. Rev. Lett.* **87** 086401 (2001)
[25] Kravchenko S V, Shashkin A A, Dolgopolov V T *Phys. Rev. Lett.* **89** 219701 (2002)
[26] Gao X P A, Mills A P Jr., Ramirez A P, Pfeiffer L N, West K W *Phys. Rev. Lett.* **89** 016801 (2002)
[27] Zhu J, Stormer H L, Pfeiffer L N, Baldwin K W, West K W *Phys. Rev. Lett.* **90** 056805 (2003)
[28] Shashkin A A, Kravchenko S V, Dolgopolov V T, Klapwijk T M *Phys. Rev. B* **66** 073303 (2002)
[29] Shashkin A A, Rahimi M, Anissimova S, Kravchenko S V, Dolgopolov V T, Klapwijk T M *Phys. Rev. Lett.* **91** 046403 (2003)
[30] Shashkin A A, Kravchenko S V, Dolgopolov V T, Klapwijk T M *J. Phys. A: Math. Gen.* **36** 9237 (2003)
[31] Abrahams E, Kravchenko S V, Sarachik M P *Rev. Mod. Phys.* **73** 251 (2001)

[32] Kravchenko S V, Sarachik M P *Rep. Prog. Phys.* **67** 1 (2004)
[33] Lozovik Y E, Yudson V I *JETP Lett.* **22** 11 (1975)
[34] Tsukada M *J. Phys. Soc. Jpn.* **42** 391 (1977)
[35] Maki K, Zotos X *Phys. Rev. B* **28** 4349 (1983)
[36] Lam P K, Girvin S M *Phys. Rev. B* **30** 473 (1984)
[37] Levesque D, Weiss J J, MacDonald A M *Phys. Rev. B* **30** 1056 (1984)
[38] D'Iorio M, Pudalov V M, Semenchinsky S G *Phys. Lett. A* **150** 422 (1990)
[39] Kravchenko S V, Perenboom J A A J, Pudalov V M *Phys. Rev. B* **44** 13513 (1991)
[40] D'Iorio M, Pudalov V M, Semenchinsky S G *Phys. Rev. B* **46** 15992 (1992)
[41] Pudalov V M, D'Iorio M, Kravchenko S V, Campbell J W *Phys. Rev. Lett.* **70** 1866 (1993)
[42] Willett R L, Stormer H L, Tsui D C, Pfeiffer L N, West K W, Baldwin K W *Phys. Rev. B* **38** 7881 (1988)
[43] Goldman V J, Shayegan M, Tsui D C *Phys. Rev. Lett.* **61** 881 (1988)
[44] Andrei E Y, Deville G, Glattli D C, Williams F I B, Paris E, Etienne B *Phys. Rev. Lett.* **60** 2765 (1988)
[45] Willett R L, Stormer H L, Tsui D C, Pfeiffer L N, West K W, Shayegan M, Santos M, Sajoto T *Phys. Rev. B* **40** 6432 (1989)
[46] Jiang H W, Willett R L, Stormer H L, Tsui D C, Pfeiffer L N, West K W *Phys. Rev. Lett.* **65** 633 (1990)
[47] Goldman V J, Santos M, Shayegan M, Cunningham J E *Phys. Rev. Lett.* **65** 2189 (1990)
[48] Williams F I B, Wright P A, Clark R G, Andrei E Y, Deville G, Glattli D C, Probst O, Etienne B, Dorin C, Foxon C T, Harris J J *Phys. Rev. Lett.* **66** 3285 (1991)
[49] Jiang H W, Stormer H L, Tsui D C, Pfeiffer L N, West K W *Phys. Rev. B* **44** 8107 (1991)
[50] Santos M B, Suen Y W, Shayegan M, Li Y P, Engel L W, Tsui D C *Phys. Rev. Lett.* **68** 1188 (1992)
[51] Santos M B, Jo J, Suen Y W, Engel L W, Shayegan M *Phys. Rev. B* **46** 13639 (1992)
[52] Manoharan H C, Shayegan M *Phys. Rev. B* **50** 17662 (1994)
[53] von Klitzing K, Dorda G, Pepper M *Phys. Rev. Lett.* **45** 494 (1980)
[54] Kivelson S A, Lee D H, Zhang S C *Phys. Rev. B* **46** 2223 (1992)
[55] Khmelnitskii D E *Helv. Phys. Acta* **65** 164 (1992)
[56] Huckestein B *Phys. Rev. Lett.* **84** 3141 (2000)
[57] Dolgopolov V T, Kravchenko G V, Shashkin A A, Kravchenko S V *Phys. Rev. B* **46** 13303 (1992)
[58] Kravchenko S V, Mason W, Furneaux J E, Pudalov V M *Phys. Rev. Lett.* **75** 910 (1995)
[59] Dultz S C, Jiang H W, Schaff W J *Phys. Rev. B* **58** R7532 (1998)
[60] Hilke M, Shahar D, Song S H, Tsui D C, Xie Y H *Phys. Rev. B* **62** 6940 (2000)
[61] Glozman I, Johnson C E, Jiang H W *Phys. Rev. Lett.* **74** 594 (1995)
[62] Shashkin A A, Kravchenko G V, Dolgopolov V T, Kravchenko S V, Furneaux J E *Phys. Rev. Lett.* **75** 2248 (1995)
[63] Pudalov V M, D'Iorio M, Campbell J W *JETP Lett.* **57** 608 (1993)
[64] Jiang H W, Johnson C E, Wang K L, Hannahs S T *Phys. Rev. Lett.* **71** 1439 (1993)
[65] Shahar D, Tsui D C, Cunningham J E *Phys. Rev. B* **52** R14372 (1995)
[66] Hilke M, Shahar D, Song S H, Tsui D C, Xie Y H, Monroe D *Phys. Rev. B* **56** R15545 (1997)
[67] Sakr M R, Rahimi M, Kravchenko S V, Coleridge P T, Williams R L, Lapointe J *Phys. Rev. B* **64** 161308(R) (2001)
[68] Wang T, Clark K P, Spencer G F, Mack A M, Kirk W P *Phys. Rev. Lett.* **72** 709 (1994)
[69] Hughes R J F, Nicholls J T, Frost J E F, Linfield E H, Pepper M, Ford C J B, Ritchie D A, Jones G A C, Kogan E, Kaveh M *J. Phys. Condens. Matter* **6** 4763 (1994)
[70] Song S H, Shahar D, Tsui D C, Xie Y H, Monroe D *Phys. Rev. Lett.* **78** 2200 (1997)
[71] Lee C H, Chang Y H, Suen Y W, Lin H H *Phys. Rev. B* **58** 10629 (1998)
[72] Hilke M, Shahar D, Song S H, Tsui D C, Xie Y H, Monroe D *Nature* **395** 675 (1998)
[73] Hilke M, Shahar D, Song S H, Tsui D C, Xie Y H, Shayegan M *Europhys. Lett.* **46** 775 (1999)
[74] Hanein Y, Nenadovic N, Shahar D, Shtrikman H, Yoon I, Li C C, Tsui D C *Nature* **400** 735 (1999)
[75] Popović D, Fowler A B, Washburn S *Phys. Rev. Lett.* **79** 1543 (1997)
[76] Coleridge P T, Williams R L, Feng Y, Zawadzki P *Phys. Rev. B* **56** R12764 (1997)
[77] Shashkin A A, Kravchenko S V, Klapwijk T M *Phys. Rev. Lett.* **87** 266402 (2001)
[78] Papadakis S J, Shayegan M *Phys. Rev. B* **57** R15068 (1998)
[79] Hanein Y, Meirav U, Shahar D, Li C C, Tsui D C, Shtrikman H *Phys. Rev. Lett.* **80** 1288 (1998)
[80] Simmons M Y, Hamilton A R, Pepper M, Linfield E H, Rose P D, Ritchie D A, Savchenko A K, Griffiths T G *Phys. Rev. Lett.* **80** 1292 (1998)
[81] Mills A P Jr., Ramirez A P, Pfeiffer L N, West K W *Phys. Rev. Lett.* **83** 2805 (1999)
[82] Yoon J, Li C C, Shahar D, Tsui D C, Shayegan M *Phys. Rev. Lett.* **82** 1744 (1999)
[83] Simmons M Y, Hamilton A R, Pepper M, Linfield E H, Rose P D, Ritchie D A *Phys. Rev. Lett.* **84** 2489 (2000)
[84] Noh H, Lilly M P, Tsui D C, Simmons J A, Hwang E H, Das Sarma S, Pfeiffer L N, West K W *Phys. Rev. B* **68** 165308 (2003)
[85] Pudalov V M, Brunthaler G, Prinz A, Bauer G, cond-mat/0103087
[86] Fogler M M, Shklovskii B I *Phys. Rev. B* **52** 17366 (1995)
[87] Tikofsky A M, Kivelson S A *Phys. Rev. B* **53** R13275 (2000)
[88] Ando T *J. Phys. Soc. Jpn.* **53** 3126 (1984)
[89] Shahbazyan T V, Raikh M E *Phys. Rev. Lett.* **75** 304 (1995)
[90] Kagalovsky V, Horovitz B, Avishai Y *Phys. Rev. B* **52** R17044 (1995)
[91] Gramada A, Raikh M E *Phys. Rev. B* **54** 1928 (1996)
[92] Haldane F D M, Yang K *Phys. Rev. Lett.* **78** 298 (1997)
[93] Fogler M M *Phys. Rev. B* **57** 11947 (1998)
[94] Liu D Z, Xie X C, Niu Q *Phys. Rev. Lett.* **76** 975 (1996)
[95] Xie X C, Liu D Z, Sundaram B, Niu Q *Phys. Rev. B* **54** 4966 (1996)
[96] Hatsugai Y, Ishibashi K, Morita Y *Phys. Rev. Lett.* **83** 2246 (1999)
[97] Yang K, Bhatt R N *Phys. Rev. Lett.* **76** 1316 (1996)
[98] Yang K, Bhatt R N *Phys. Rev. B* **59** 8144 (1999)
[99] Koschny T, Potempa H, Schweitzer L *Phys. Rev. Lett.*

**86** 3863 (2001)
[100] Pereira A L C, Schulz P A *Phys. Rev. B* **66** 155323 (2002)
[101] Koschny T, Schweitzer L *Phys. Rev. B* **67** 195307 (2003)
[102] Sheng D N, Weng Z Y *Phys. Rev. Lett.* **78** 318 (1997)
[103] Sheng D N, Weng Z Y *Phys. Rev. B* **62** 15363 (2000)
[104] Okamoto T, Shinohara Y, Kawaji S *Phys. Rev. B* **52** 11109 (1995)
[105] Dultz S C, Jiang H W *Phys. Rev. Lett.* **84** 4689 (2000)
[106] Fogler M M *Phys. Rev. B* **69** 121409(R) (2004)
[107] Dolgopolov V T, Kravchenko G V, Shashkin A A *JETP Lett.* **55** 140 (1992)
[108] Dolgopolov V T, Kravchenko G V, Shashkin A A, Kravchenko S V *JETP Lett.* **55** 733 (1992)
[109] Dolgopolov V T, Shashkin A A, Kravchenko G V, Emeleus C J, Whall T E *JETP Lett.* **62** 168 (1995)
[110] Adkins C J, Pollitt S, Pepper M *J. Phys. C* **37** 343 (1976)
[111] Polyakov D G, Shklovskii B I *Phys. Rev. B* **48** 11167 (1993)
[112] Shklovskii B I, Efros A L *Electronic Properties of Doped Semiconductors* (Springer, New York, 1984)
[113] Li Y P, PhD thesis, Princeton University, 1994
[114] Kukushkin I V, Timofeev V B *Sov. Phys. Usp.* **36** 549 (1993)
[115] Iordansky S V *Solid State Commun.* **43** 1 (1982)
[116] Ando T *J. Phys. Soc. Jpn.* **52** 1740 (1983)
[117] Aoki H *J. Phys. C* **16** 1893 (1983)
[118] Aoki H, Ando T *Phys. Rev. Lett.* **54** 831 (1985)
[119] Pruisken A M M *Phys. Rev. Lett.* **61** 1297 (1988)
[120] Wei H P, Tsui D C, Paalanen M A, Pruisken A M M *Phys. Rev. Lett.* **61** 1294 (1988)
[121] Wakabayashi J, Yamane M, Kawaji S *J. Phys. Soc. Jpn.* **58** 1903 (1989)
[122] Koch S, Haug R J, von Klitzing K, Ploog K *Phys. Rev. B* **43** 6828 (1991)
[123] Dolgopolov V T, Shashkin A A, Medvedev B K, Mokerov V G *Sov. Phys. JETP* **72** 113 (1991)
[124] Koch S, Haug R J, von Klitzing K, Ploog K *Phys. Rev. Lett.* **67** 883 (1991)
[125] Koch S, Haug R J, von Klitzing K, Ploog K *Phys. Rev. B* **46** 1596 (1992)
[126] Wei H P, Lin S Y, Tsui D C, Pruisken A M M *Phys. Rev. B* **45** 3926 (1992)
[127] Hwang S W, Wei H P, Engel L W, Tsui D C, Pruisken A M M *Phys. Rev. B* **48** 11416 (1993)
[128] Engel L W, Shahar D, Kurdak C, Tsui D C *Phys. Rev. Lett.* **71** 2638 (1993)
[129] Wei H P, Engel L W, Tsui D C *Phys. Rev. B* **50** 14609 (1994)
[130] Wong L W, Jiang H W, Trivedi N, Palm E *Phys. Rev. B* **51** 18033 (1995)
[131] Shahar D, Tsui D C, Shayegan M, Bhatt R N, Cunningham J E *Phys. Rev. Lett.* **74** 4511 (1995)
[132] Pan W, Shahar D, Tsui D C, Wei H P, Razeghi M *Phys. Rev. B* **55** 15431 (1997)
[133] Shahar D, Tsui D C, Shayegan M, Shimshoni E, Sondhi S L *Phys. Rev. Lett.* **79** 479 (1997)
[134] Coleridge P T *Phys. Rev. B* **60** 4493 (1999)
[135] van Schaijk R T F, de Visser A, Olsthoorn S M, Wei H P, Pruisken A M M *Phys. Rev. Lett.* **84** 1567 (2000)
[136] Dunford R B, Griffin N, Pepper M, Phillips P J, Whall T E *Physica E* **6** 297 (2000)
[137] Dunford R B, Griffin N, Phillips P J, Whall T E *Physica B* **298** 496 (2001)
[138] Hohls F, Zeitler U, Haug R J *Phys. Rev. Lett.* **86** 5124 (2001)
[139] Hohls F, Zeitler U, Haug R J *Phys. Rev. Lett.* **88** 036802 (2002)
[140] Hohls F, Zeitler U, Haug R J, Meisels R, Dybko K, Kuchar F *Phys. Rev. Lett.* **89** 276801 (2002)
[141] Balaban N Q, Meirav U, Bar-Joseph I *Phys. Rev. Lett.* **81** 4967 (1998)
[142] Shahar D, Hilke M, Li C C, Tsui D C, Sondhi S L, Cunningham J E, Razeghi M *Solid State Commun.* **107** 19 (1998)
[143] Arapov Y G, Alshanskii G A, Harus G I, Neverov V N, Shelushinina N G, Yakunin M V, Kuznetsov O A *Nanotechnology* **13** 86 (2002)
[144] Huckestein B *Rev. Mod. Phys.* **67** 357 (1995)
[145] Wysokinski K I, Brenig W *Z. Phys. B* **54** 11 (1983)
[146] Viehweger O, Efetov K B *J. Phys. Condens. Matter* **2** 7049 (1990)
[147] Viehweger O, Efetov K B *Phys. Rev. B* **44** 1168 (1991)
[148] Zhang S C, Kivelson S, Lee D H *Phys. Rev. Lett.* **69** 1252 (1992)
[149] Wakabayashi J, Fukano A, Kawaji S, Hirakawa K, Sakaki H, Koike Y, Fukase T *J. Phys. Soc. Jpn.* **57** 3678 (1988)
[150] Dorozhkin S I, Shashkin A A, Kravchenko G V, Dolgopolov V T, Haug R J, von Klitzing K, Ploog K *JETP Lett.* **57** 58 (1993)
[151] Goldman V J, Wang J K, Su B, Shayegan M *Phys. Rev. Lett.* **70** 647 (1993)
[152] Sajoto T, Li Y P, Engel L W, Tsui D C, Shayegan M *Phys. Rev. Lett.* **70** 2321 (1993)
[153] Kravchenko S V, Furneaux J E, Pudalov V M *Phys. Rev. B* **49** 2250 (1994)
[154] Pudalov V M, D'Iorio M, Campbell J W *Surf. Sci.* **305** 107 (1994)
[155] Levine H, Libby S B, Pruisken A M M *Phys. Rev. Lett.* **51** 1915 (1983)
[156] Khmelnitskii D E *JETP Lett.* **38** 552 (1983)
[157] Dykhne A M, Ruzin I M *Phys. Rev. B* **50** 2369 (1994)
[158] Ruzin I, Feng S *Phys. Rev. Lett.* **74** 154 (1995)
[159] Burgess C P, Dib R, Dolan B P *Phys. Rev. B* **62** 15359 (2000)
[160] Wei H P, Tsui D C, Pruisken A M M *Phys. Rev. B* **33** 1488 (1986)
[161] Halperin B I *Phys. Rev. B* **25** 2185 (1982)
[162] *The Quantum Hall Effect* Ed. by Prange R E, Girvin S M (Springer-Verlag, 1987)
[163] Büttiker M *Phys. Rev. B* **38** 9375 (1988)
[164] Laughlin R B *Phys. Rev. B* **23** 5632 (1981)
[165] Widom A, Clark T D *J. Phys. D* **15** L181 (1982)
[166] Dolgopolov V T, Zhitenev N B, Shashkin A A *JETP Lett.* **52** 196 (1990)
[167] Dolgopolov V T, Zhitenev N B, Shashkin A A *Europhys. Lett.* **14** 255 (1991)
[168] Dolgopolov V T, Shashkin A A, Zhitenev N B, Dorozhkin S I, von Klitzing K *Phys. Rev. B* **46** 12560 (1992)
[169] Dolgopolov V T, Shashkin A A, Kravchenko G V, Dorozhkin S I, von Klitzing K *Phys. Rev. B* **48** 8480 (1993)
[170] Jeanneret B, Hall B D, Buhlmann H J, Houdre R, Ilegems M, Jeckelmann B, Feller U *Phys. Rev. B* **51** 9752 (1995)
[171] Watts J P, Usher A, Matthews A J, Zhu M, Elliott

M, Herrenden-Harker W G, Morris P R, Simmons M Y, Ritchie D A *Phys. Rev. Lett.* **81** 4220 (1998)
[172] Honold M M, Harrison N, Singleton J, Nam M S, Blundell S J, Mielke C H, Kartsovnik M V, Kushch N D *Phys. Rev. B* **59** R10417 (1999)
[173] Dolgopolov V T, Shashkin A A, Broto J M, Rakoto H, Askenazy S *Phys. Rev. Lett.* **86** 5566 (2001)
[174] Dolgopolov V T, Kravchenko G V, Shashkin A A *Solid State Commun.* **78** 999 (1991)
[175] Haug R J *Semicond. Sci. Technol.* **8** 131 (1993)
[176] Fontein P F, Kleinen J A, Hendriks P, Blom F A P, Wolter J H, Lochs H G M, Driessen F A J M, Giling L J, Beenakker C W J *Phys. Rev. B* **43** 12090 (1991)
[177] Kent A J, McKitterick D J, Challis L J, Hawker P, Mellor C J, Henini M *Phys. Rev. Lett.* **69** 1684 (1992)
[178] Merz R, Keilmann F, Haug R J, Ploog K *Phys. Rev. Lett.* **70** 651 (1993)
[179] Shashkin A A, Kent A J, Harrison P A, Strickland K R, Eaves L, Henini M *Semicond. Sci. Technol.* **9** 2110 (1994)
[180] Shashkin A A, Kent A J, Harrison P A, Eaves L, Henini M *Phys. Rev. B* **49** 5379 (1994)
[181] van Haren R J F, Blom F A P, Wolter J H *Phys. Rev. Lett.* **74** 1198 (1995)
[182] van Haren R J F, de Lange W, Blom F A P, Wolter J H *Phys. Rev. B* **52** 5760 (1995)
[183] Shashkin A A, Kent A J, Owers-Bradley J R, Cross A J, Hawker P, Henini M *Phys. Rev. Lett.* **79** 5114 (1997)
[184] Wei Y Y, Weis J, von Klitzing K, Eberl K *Phys. Rev. Lett.* **81** 1674 (1998)
[185] Tessmer S H, Glicofridis P I, Ashoori R C, Levitov L S, Melloch M R *Nature* **392** 51 (1998)
[186] McCormick K L, Woodside M T, Huang M, Wu M, McEuen P L, Duruoz C, Harris J S Jr. *Phys. Rev. B* **59** 4654 (1999)
[187] Yacoby A, Hess H F, Fulton T A, Pfeiffer L N, West K W *Solid State Commun.* **111** 1 (1999)
[188] Shashkin A A, Kent A J, Hawker P, Henini M *Phys. Rev. B* **60** R16307 (1999)
[189] Zhitenev N B, Fulton T A, Yacoby A, Hess H F, Pfeiffer L N, West K W *Nature* **404** 473 (2000)
[190] Finkelstein G, Glicofridis P I, Ashoori R C, Shayegan M *Science* **289** 90 (2000)
[191] Finkelstein G, Glicofridis P I, Tessmer S H, Ashoori R C, Melloch M R *Phys. Rev. B* **61** R16323 (2000)
[192] Woodside M T, Vale C, McEuen P L, Kadow C, Maranowski K D, Gossard A C *Phys. Rev. B* **64** 041310(R) (2001)
[193] van Zalinge H, Özyilmaz B, Böhm A, van der Heijden R W, Wolter J H, Wyder P *Phys. Rev. B* **64** 235303 (2001)
[194] Glicofridis P I, Finkelstein G, Ashoori R C, Shayegan M *Phys. Rev. B* **65** 121312(R) (2002)
[195] Chklovskii D B, Shklovskii B I, Glazman L I *Phys. Rev. B* **46** 4026 (1992)
[196] Ebert G, von Klitzing K, Weimann G *J. Phys. C* **18** L257 (1985)
[197] Pudalov V M, Semenchinskii S G *JETP Lett.* **42** 232 (1985)
[198] Shashkin A A, Dolgopolov V T, Dorozhkin S I *Sov. Phys. JETP* **64** 1124 (1986)
[199] Wiegers S A J, Lok J G S, Jeuken M, Zeitler U, Maan J C, Henini M *Phys. Rev. B* **59** 7323 (1999)
[200] Sarachik M P, Kravchenko S V *Proc. Natl. Acad. Sci. USA* **96** 5900 (1999)
[201] Kravchenko S V, Klapwijk T M *Phys. Rev. Lett.* **84** 2909 (2000)
[202] Jaroszyński J, Popović D, Klapwijk T M *Phys. Rev. Lett.* **89** 276401 (2002)
[203] Simonian D, Kravchenko S V, Sarachik M P *Phys. Rev. B* **55** R13421 (1997)
[204] Okamoto T, Hosoya K, Kawaji S, Yagi A *Phys. Rev. Lett.* **82** 3875 (1999)
[205] Vitkalov S A, Zheng H, Mertes K M, Sarachik M P, Klapwijk T M *Phys. Rev. Lett.* **85** 2164 (2000)
[206] Vitkalov S A, Sarachik M P, Klapwijk T M *Phys. Rev. B* **64** 073101 (2001)
[207] Bogdanovich S, Popović D *Phys. Rev. Lett.* **88** 236401 (2002)
[208] Leturcq R, L'Hote D, Tourbot R, Mellor C J, Henini M *Phys. Rev. Lett.* **90** 076402 (2003)
[209] Stern F *Phys. Rev. Lett.* **44** 1469 (1980)
[210] Gold A, Dolgopolov V T *Phys. Rev. B* **33** 1076 (1986)
[211] Das Sarma S *Phys. Rev. B* **33** 5401 (1986)
[212] Das Sarma S, Hwang E H *Phys. Rev. Lett.* **83** 164 (1999)
[213] Fang F F, Stiles P J *Phys. Rev.* **174** 823 (1968)
[214] Smith J L, Stiles P J *Phys. Rev. Lett.* **29** 102 (1972)
[215] Ando T, Uemura Y *J. Phys. Soc. Jpn.* **37** 1044 (1974)
[216] Bychkov Yu A, Iordanskii S V, Eliashberg G M *JETP Lett.* **33** 143 (1981)
[217] Kallin C, Halperin B I *Phys. Rev. B* **30** 5655 (1984)
[218] MacDonald A H, Oji H C A, Liu K L *Phys. Rev. B* **34** 2681 (1986)
[219] Smith A P, MacDonald A H, Gumbs G *Phys. Rev. B* **45** 8829 (1992)
[220] Simonian D, Kravchenko S V, Sarachik M P, Pudalov V M *Phys. Rev. Lett.* **79** 2304 (1997)
[221] Pudalov V M, Brunthaler G, Prinz A, Bauer G *JETP Lett.* **65** 932 (1997)
[222] Pudalov V M, Brunthaler G, Prinz A, Bauer G *Phys. Rev. Lett.* **88** 076401 (2002)
[223] Dolgopolov V T, Gold A *JETP Lett.* **71** 27 (2000)
[224] Pudalov V M, Gershenson M E, Kojima H, Butch N, Dizhur E M, Brunthaler G, Prinz A, Bauer G *Phys. Rev. Lett.* **88** 196404 (2002)
[225] Vitkalov S A, Sarachik M P, Klapwijk T M *Phys. Rev. B* **65** 201106(R) (2002)
[226] Sarachik M P, Vitkalov S A *J. Phys. Soc. Jpn.* **72** 57 (2003)
[227] Prus O, Yaish Y, Reznikov M, Sivan U, Pudalov V *Phys. Rev. B* **67** 205407 (2003)
[228] Dolgopolov V T, Gold A *Phys. Rev. Lett.* **89** 129701 (2002)
[229] Gold A, Dolgopolov V T *J. Phys.: Condens. Matter* **14** 7091 (2002)
[230] Batke E, Tu C W *Phys. Rev. B* **34** 3027 (1986)
[231] Das Sarma S, Hwang E H *Phys. Rev. Lett.* **84** 5596 (2000)
[232] Tutuc E, Melinte S, Shayegan M *Phys. Rev. Lett.* **88** 036805 (2002)
[233] Noh H, Lilly M P, Tsui D C, Simmons J A, Hwang E H, Das Sarma S, Pfeiffer L N, West K W *Phys. Rev. B* **68** 165308 (2002)
[234] Tutuc E, Melinte S, De Poortere E P, Shayegan M, Winkler R *Phys. Rev. B* **67** 241309(R) (2003)
[235] Vakili K, Shkolnikov Y P, Tutuc E, De Poortere E P, Shayegan M *Phys. Rev. Lett.* **92** 226401 (2004)
[236] Dolgopolov V T, Deviatov E V, Shashkin A A, Wieser U, Kunze U, Abstreiter G, Brunner K *Superlattices Mi-*

*crostruct.* **33** 271 (2003)
[237] Okamoto T, Ooya M, Hosoya K, Kawaji S *Phys. Rev. B* **69** 041202 (2004)
[238] Zala G, Narozhny B N, Aleiner I L *Phys. Rev. B* **64** 214204 (2001)
[239] Ando T, Fowler A B, Stern F *Rev. Mod. Phys.* **54** 437 (1982)
[240] Iwamoto N *Phys. Rev. B* **43** 2174 (1991)
[241] Kwon Y, Ceperley D M, Martin R M *Phys. Rev. B* **50** 1684 (1994)
[242] Chen G H, Raikh M E *Phys. Rev. B* **60** 4826 (1999)
[243] Proskuryakov Y Y, Savchenko A K, Safonov S S, Pepper M, Simmons M Y, Ritchie D A *Phys. Rev. Lett.* **89** 076406 (2002)
[244] Coleridge P T, Sachrajda A S, Zawadzki P *Phys. Rev. B* **65** 125328 (2002)
[245] Vitkalov S A, James K, Narozhny B N, Sarachik M P, Klapwijk T M *Phys. Rev. B* **67** 113310 (2003)
[246] Pudalov V M, Gershenson M E, Kojima H, Brunthaler G, Prinz A, Bauer G *Phys. Rev. Lett.* **91** 126403 (2003)
[247] Das Sarma S, Hwang E H *Phys. Rev. Lett.* **93** 269703 (2004)
[248] Shashkin A A, Dolgopolov V T, Kravchenko S V *Phys. Rev. Lett.* **93** 269705 (2004)
[249] Martin G W, Maslov D L, Reizer M Yu *Phys. Rev. B* **68** 241309(R) (2003)
[250] Shkolnikov Y P, Vakili K, De Poortere E P, Shayegan M *Phys. Rev. Lett.* **92** 246804 (2004)
[251] Smith T P, Goldberg B B, Stiles P J, Heiblum M *Phys. Rev. B* **32** 2696 (1985)
[252] Pudalov V M, Semenchinskii S G *JETP Lett.* **44** 677 (1986)
[253] Khrapai V S, Shashkin A A, Dolgopolov V T *Phys. Rev. B* **67** 113305 (2003)
[254] Khrapai V S, Shashkin A A, Dolgopolov V T *Phys. Rev. Lett.* **91** 126404 (2003)
[255] Usher A, Nicholas R J, Harris J J, Foxon C T *Phys. Rev. B* **41** 1129 (1990)
[256] Dolgopolov V T, Shashkin A A, Aristov A V, Schmerek D, Hansen W, Kotthaus J P, Holland M *Phys. Rev. Lett.* **79** 729 (1997)
[257] Spivak B *Phys. Rev. B* **67** 125205 (2003)
[258] Spivak B *Phys. Rev. B* **64** 085317 (2001)
[259] Brinkman W F, Rice T M *Phys. Rev. B* **2** 4302 (1970)
[260] Dolgopolov V T *JETP Lett.* **76** 377 (2002)
[261] Tanasković D, Dobrosavljević V, Abrahams E, Kotliar G *Phys. Rev. Lett.* **91** 066603 (2003)
[262] Dharma-wardana M W C *Europhys. Lett.* **67** 552 (2004)
[263] Dharma-wardana M W C, Perrot F *Phys. Rev. B* **70** 035308 (2004)
[264] Khodel V A, Shaginyan V R *JETP Lett.* **51** 553 (1990)
[265] Asgari R, Davoudi B, Tanatar B *Solid State Commun.* **130** 13 (2004)